Rockwell International

Rockwell International

Rocketdyne Division
6633 Canoga Avenue
Canoga Park, California 91304

NON-INTRUSIVE SPEED SENSOR

NAS8-34658

FINAL REPORT

PHASE I

RI/RD84-232

OCTOBER, 1984

PREPARED FOR:
NASA-MARSHALL SPACE FLIGHT CENTER

HUNTSVILLE, ALABAMA 35812

PREPARED BY

L. WYETT/J. MARAM
MEMBERS OF TECHNICAL STAFF
ADVANCED INSTRUMENTATION

APPROVED BY

S. BARKHOUDARIAN
PROJECT ENGINEER
ADVANCED INSTRUMENTATION

G. F. BREMER
PROJECT MANAGER
ADVANCED BOOSTER PROPULSION

ABSTRACT

A computerized literature search was performed to identify candidate technologies for remote, non-intrusive speed sensing applications in Space Shuttle Main Engine (SSME) turbopumps. The three most promising technologies were subjected to experimental evaluation to quantify their performance characteristics under the harsh environmental requirements within the turbopumps. Although the infrared and microwave approaches demonstrated excellent cavitation immunity in laboratory tests, the variable-source magnetic speed sensor emerged as the most viable approach. Preliminary design of this speed sensor has encountered no technical obstacles and has resulted in viable and feasible speed nut, sensor housing, and sensor coil designs.

SUMMARY

A computerized literature search on non-intrusive/non-contacting speed sensing technologies was performed, resulting in 550 abstracts and 42 articles. Fourteen techniques were identified and theoretically analyzed, resulting in the recommendation of the Microwave, Infrared, and Magnetic technologies for experimental evaluation.

Experimental studies of the effects of induced cavitation on the transmittance of liquid media at standard temperature and pressure have shown that both infrared and microwave wavelength bands can be utilized in non-intrusive speed sensors. Final verification of these approaches would be necessary under the cryogenic, high pressure conditions that exist inside an operating HPOTP.

Test results with a variable-source magnetic approach, consisting of permanent magnets placed on the rotating shaft and a pickup coil placed on the housing, indicated detection of a strong signal from 3.5 inches at the lowest required speed. The preliminary design of this variable-source magnetic speed sensor encountered no technical obstacles and has resulted in viable and feasible SSME HPOTP speed nut, sensor housing, and sensor coil designs.

INTRODUCTION

Reusable rocket engines such as the Space Shuttle Main Engines (SSME) and the Orbital Transfer Vehicles (OTV) have throttling capabilities that require real-time, closed-loop control systems of engine propellant flows, combustion temperatures and pressures, and turbopump rotary speeds. In the case of the SSME, there are four turbopumps that require real-time measurement and red-line control of their rotary speeds. Variable-reluctance magnetic speed sensors were designed, fabricated, and tested for all four turbopumps, resulting in the successful implementation and operation of three of these speed sensors during each of the 13 Shuttle flights. The fourth speed sensor, Figure 1, designed for the High Pressure Oxidizer Turbopump (HPOTP), shown in

HPOTP SPEED SENSOR

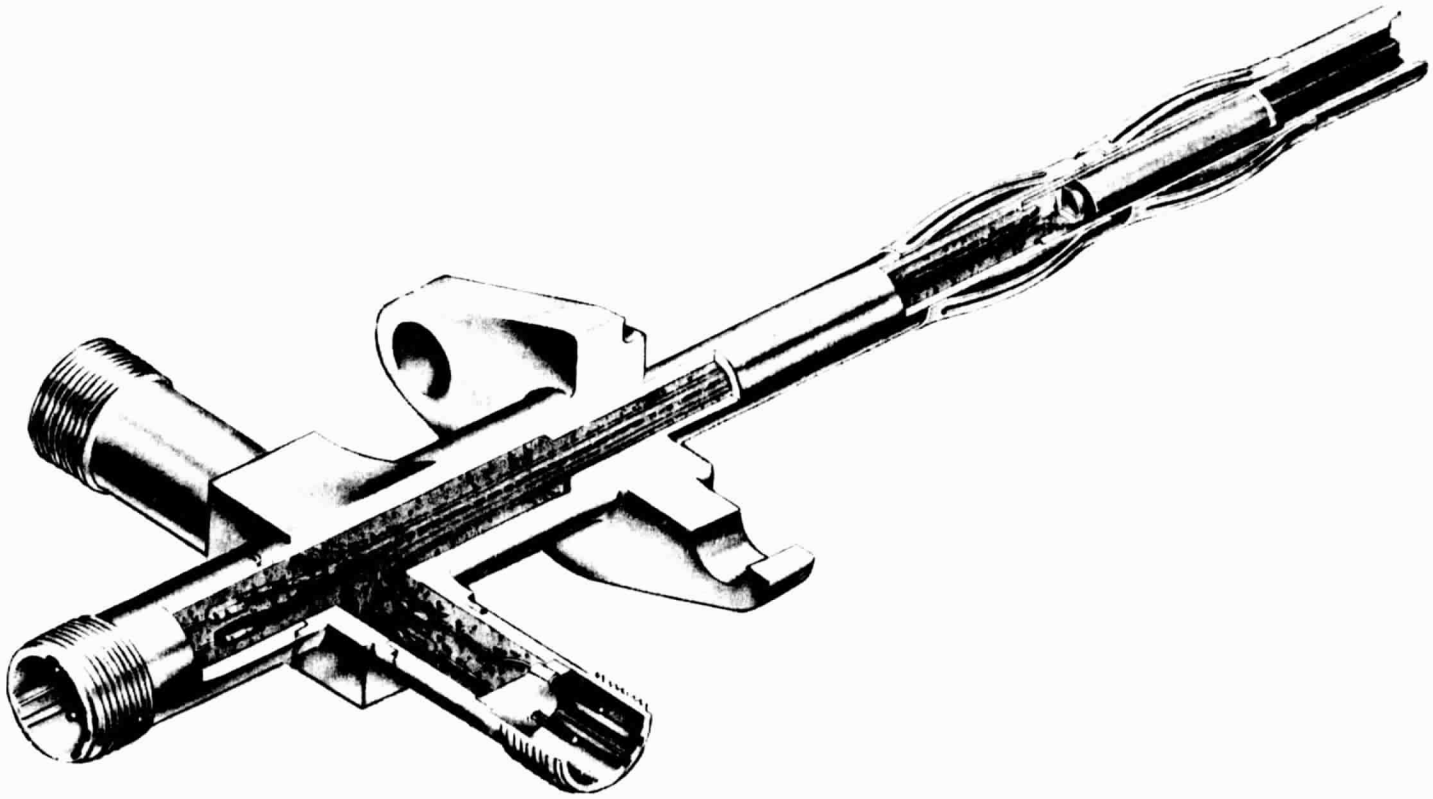

LC305-261A

Rockwell International
Rocketdyne Division

Figure 1

Figure 2, was removed from all flights and ground tests due to structural weaknesses of its 3.5-inch long intrusive probe tip, which had to withstand 200 ft/sec flow velocities and 34.5 g_{rms} vibration in a liquid-oxygen environment where loose-part collisions can have catastrophic consequences. The probe tip, shown in Figure 3, could not have been shortened because the signal amplitude would have been reduced to less than 20 microvolts at 500 rpm for a 3.5-inch separation between the speed nut and the pickup coil. This is an impractical signal level for SSME applications.

To overcome this problem, a technology program was initiated by MSFC resulting in a contract award to Rocketdyne. The timeline of this program is shown in Table 1. This program consisted of identification, analysis, experimental evaluation of non-intrusive speed measurement techniques, a tradeoff study, and preliminary design of a selected non-intrusive speed sensor capable of measuring the speed of any SSME turbopump in the range of 500 to 50,000 rpm with $\pm$25 rpm accuracy.

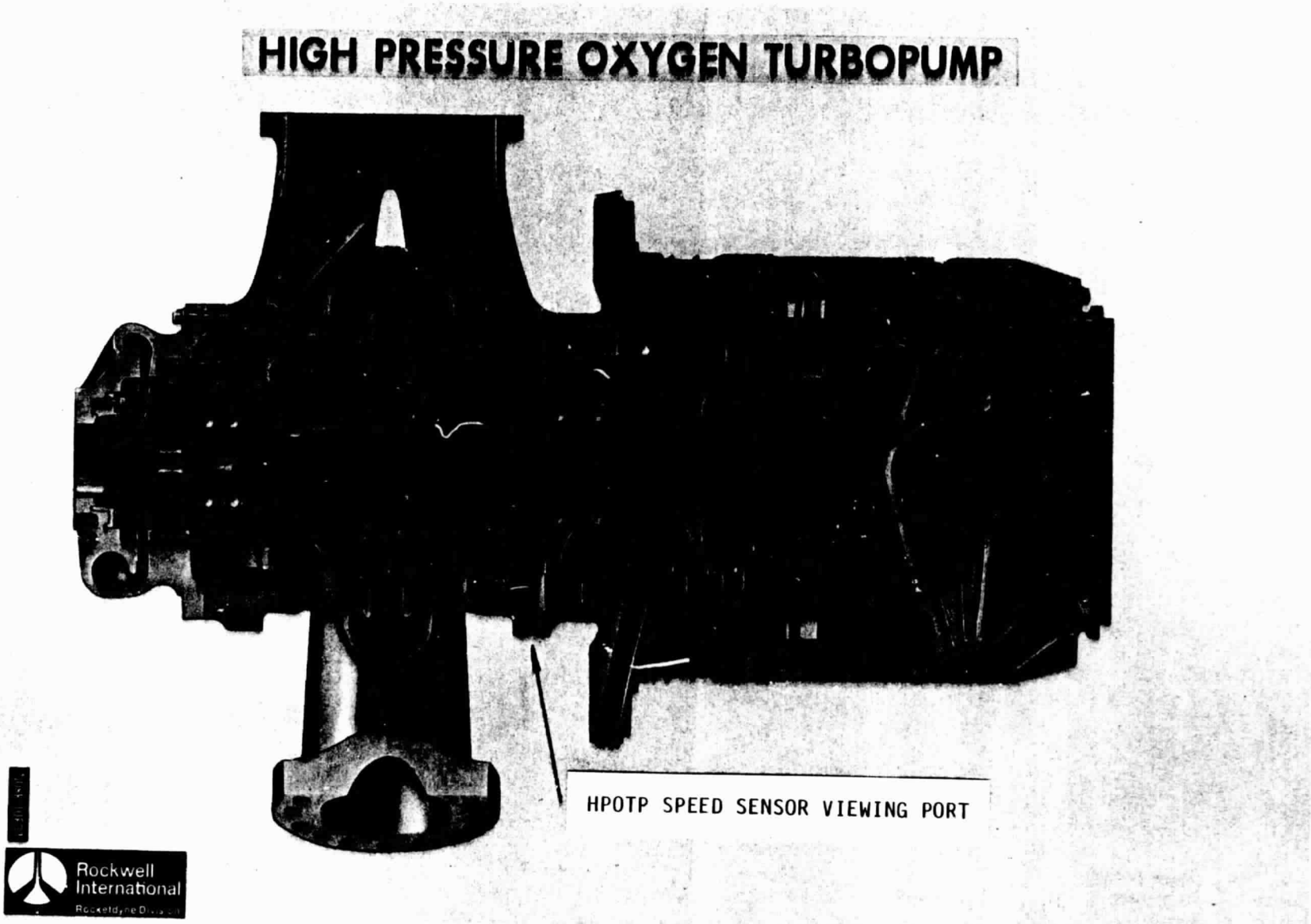
HIGH PRESSURE OXYGEN TURBOPUMP
HPOTP SPEED SENSOR VIEWING PORT
Rockwell International

Figure 2

EXISTING SSME SPEED SENSOR

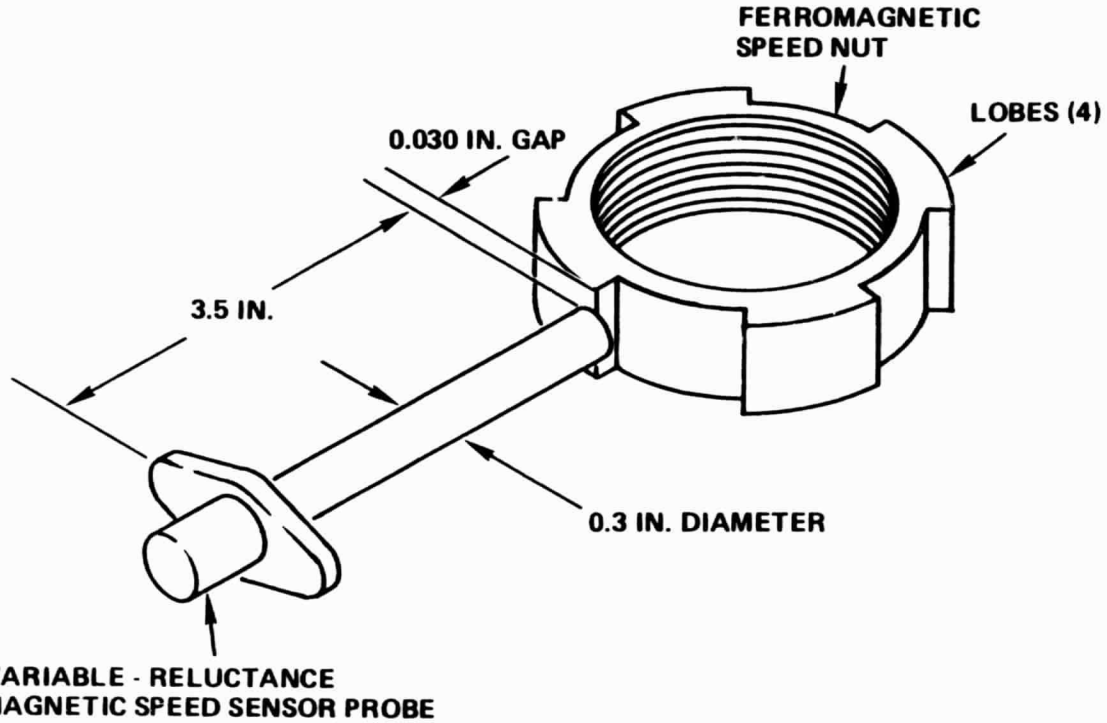

487-695

Rockwell International
Rocketdyne Division

Figure 3

TABLE 1

PROGRAM PLAN

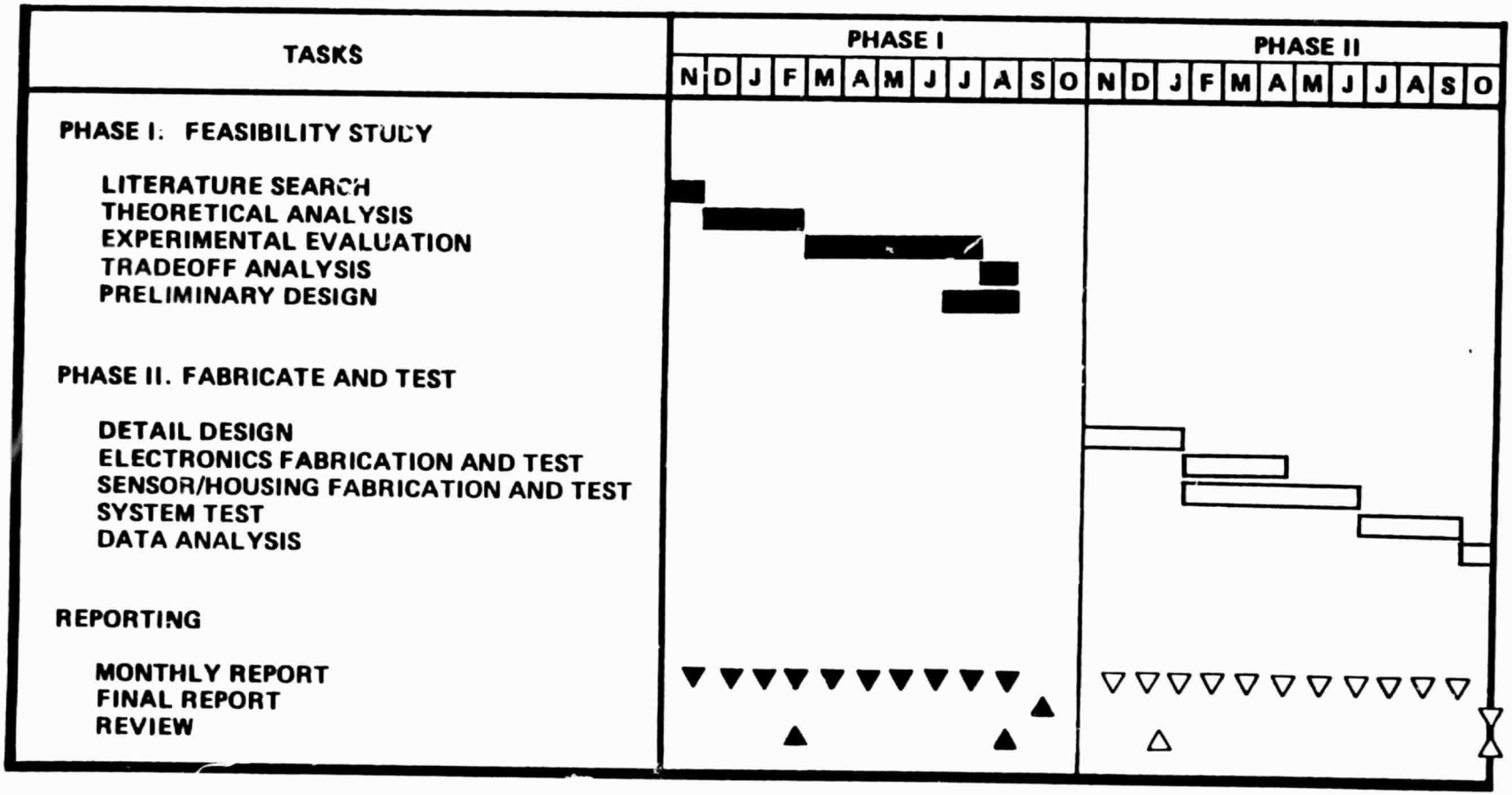

485-988

Rockwell International
Rocketdyne Division

TASK I - LITERATURE SEARCH

To identify all non-intrusive speed sensing technologies, computerized literature searches were performed to identify published articles citing keywords such as "remote," "non-intrusive", "speed", "sensor", and "measurement". These searches yielded 550 abstracts from which 42 articles were obtained for review, resulting in 6 new technologies in addition to 8 technologies already known to us, as shown in Figure 4.

These 14 candidate remote/non-intrusive speed sensing technologies, as shown in Table 2, were subjected to the subsequent theoretical and/or experimental evaluation. Each of the 14 technologies is briefly described below:

LUMPED ELECTRICAL CIRCUIT GROUP

Capacitive Speed Sensor

A capacitive speed sensor consists of a conducting plate located at the pump housing wall and a conducting speed nut. The sensor detects the varying capacitance due to variation in the separation between the plate and the rotating lobed speed nut and determines the shaft rotation speed from the repetition rate of these signals.

Eddy Current Speed Sensor

An eddy-current speed sensor consists of an energized coil at the turbopump speed sensor port and a lobed conductive speed nut on the rotating shaft. The variation in their spacing as the nut rotates generates a periodic signal in the coil. This signal could be processed to provide a measurement of shaft speed by measuring the repetition rate of these signals.

LITERATURE SEARCH

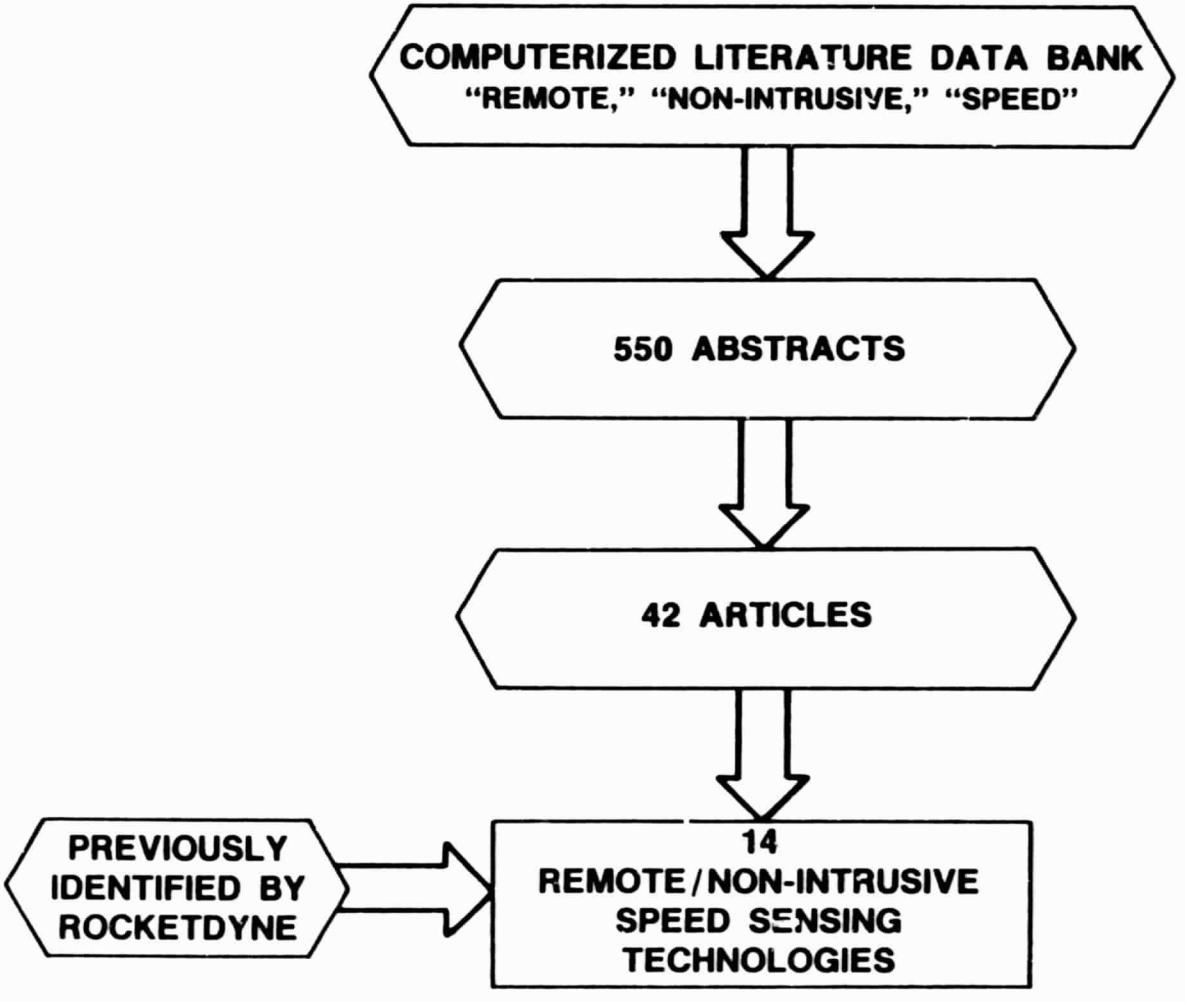

487-700

Rockwell International
Rocketdyne Division

Figure 4

TABLE 2

CANDIDATE REMOTE/NON-INTRUSIVE SPEED SENSING TECHNOLOGIES

TECHNOLOGY	ANALYSIS APPROACH	CRITICAL PARAMETER
VARIABLE-SOURCE MAGNETIC HALL-EFFECT WIEGAND-EFFECT	MAGNETICS	LOW-RPM SIGNAL AMPLITUDE
INFRARED MICROWAVE AMPLITUDE MODULATION ELECTROMAGNETIC DOPPLER SHIFT	ELECTROMAGNETIC WAVE THEORY	CAVITATION/BUBBLE ATTENUATION
ACCELEROMETER FIBEROPTIC PROXIMETER PRESSURE PULSATION ACOUSTIC	FAST FOURIER TRANSFORMS	INTERMITTENCE, LOW-RPM SIGNAL AMPLITUDE: UNRELIABLE
CAPACITANCE EDDY CURRENT ELECTROMAGNETOACOUSTIC	LUMPED ELECTRICAL CIRCUIT ELEMENTS	AMPLITUDE SENSITIVITY 1:10,000
ISOTOPE	ISOTOPES	HIGH-RPM ACCURACY

Electromagnetoacoustic Speed Sensor

An electromagnetoacoustic speed sensor consists of an array of closely spaced permanent magnets and an eddy-current induction coil. The coil, when excited with high-frequency energy, induces eddy currents in the metallic lobed speed nut. The permanent magnet array, combined with the induced current, generates in the speed nut an array of alternating force zones that creates an acoustic signal. Another similar transducer, acting as a receiver, generates a periodic electrical signal due to the varying separation between the detector and the speed nut. The repetition rate of the amplitude modulated signal can be processed to provide the measurement of the shaft speed.

FAST FOURIER TRANSFORM GROUP

Fiberoptic Proximeter Speed Sensor

A fiberoptic deflectometer consists of a fiberoptic proximity detection instrument that is inserted through a bearing housing to detect the deflection of the external surface of the bearing's outer race due to rolling balls. The fiberoptic deflectometer output signal could be processed by a Fast Fourier Transform analyzer to provide frequency information for speed measurement purposes.

Accelerometer Speed Sensor

In this approach, piezoelectric accelerometers convert turbopump-housing structural vibrations into electrical signals. For speed measurement, the signals would be processed by a Fast Fourier Transform analyzer to extract frequency information for speed measurement purposes.

Pressure Pulsation Speed Sensor

In this approach, periodic fluctuations in turbopump pressure are measured by pressure transducers and processed by a Fast Fourier Transform analyzer to extract rotational shaft speed.

Acoustic Speed Sensor

An acoustic speed sensor consists of a piezoelectric transducer emitting ultrasonic energy to a lobed speed nut, another piezoelectric transducer receiving the reflected ultrasonic energy, and an electronic system capable of processing the periodic signal whose repetition rate is proportional to the shaft speed.

ISOTOPE GROUP

Isotope Speed Sensor

An isotope speed sensor consists of a radioisotope source mounted on the speed nut and a high-energy photon detector placed on the outside of the housing. The high-energy, gamma-ray photons are detected once each time the shaft rotates and the time between successive photon bursts is measured to determine the shaft rotation speed.

MAGNETIC GROUP

Variable-Source Magnetic Speed Sensor

A variable-source magnetic speed sensor utilizes shaft-mounted, rare-earth magnets as flux generators and a non-intrusive, high-permeability pickup coil mounted at the speed sensor port at the outside of the housing. The periodic signal of such a sensor provides measurement of shaft speed.

Hall-Effect Speed Sensor

A Hall-effect speed sensor is similar to the variable-reluctance speed sensors used on the SSME, except that solid-state, Hall-effect detectors are used instead of a pickup coil for detection of magnetic field variations.

Wiegand-Effect Speed Sensor

The Wiegand-effect speed sensor is similar to the variable-reluctance speed sensor except that a Wiegand-effect core is used instead of a magnetically soft core for the pickup coil to generate a constant-amplitude signal. Such a speed sensor is presently used in commercial automotive applications.

ELECTROMAGNETIC GROUP

Infrared Speed Sensor

An infrared speed sensor consists of an infrared light-emitting diode or diode laser that directs its beam toward a speed nut encoder typically consisting of alternately polished and matted surfaces. A periodic infrared signal corresponding to the passage of the encoder surfaces is reflected back to a solid-state infrared detector. The output of the detector is processed to provide a shaft speed measurement.

Microwave Speed Sensor

A microwave signal generated by a Gunn diode is transmitted through a hollow metal waveguide and a ceramic window to a lobed speed nut. The microwave energy reflected off the speed nut is collected and processed to produce a periodic signal whose repetition rate is a measure of shaft speed.

Electromagnetic Doppler Speed Sensor

The electromagnetic Doppler approach utilizes the change in frequency observed when a microwave signal is reflected from the moving speed nut. The speed of the nut is measured directly and continuously, unlike the microwave approach discussed above. Additionally, sharp encoder lobes are not required; the surface roughness of the existing turbopump shaft may reflect sufficient microwave energy for Doppler signal detection.

TASK II - THEORETICAL ANALYSIS

Each of 14 technologies were theoretically analyzed to determine their compatibility with SSME turbopump hardware, performance, environment, and controller requirements. Those technologies that did not satisfy all the requirements were rejected. The remaining technologies were recommended for experimental evaluation. To facilitate the analysis, these 14 technologies are categorized according to the fundamental principles governing their performance. Thus, the capacitance, eddy-current, and electromagnetoacoustic speed-sensing technologies are grouped together because their performance can be evaluated by analyses of equivalent electrical lumped circuit components. The accelerometer, acoustic, pressure, and proximeter speed-sensing technologies are grouped together since their performance is dependent on the effectiveness of Fast Fourier Transform (FFT) analyses. The microwave, electromagnetic-Doppler, and infrared technologies are grouped together, the performance of each being affected by the propagation of electromagnetic waves through a cavitating liquid medium. The variable-source magnetic, Hall-effect and Wiegand-effect technologies are grouped together because their performance can be determined by analyses based on principles of magnetics.

Lumped Electrical Circuit Group Analysis

This group was analyzed for sensitivity of detection using a static lumped component representing the housing, shaft, vanes, and sensor port hole and a dynamic lumped component representing the changing gap at the speed nut periphery. All three technologies indicated a sensitivity of less than one part in ten thousand as determined from the following calculations.

The capacitance sensor configuration was simplified to represent a dynamic capacitance consisting of two port-size parallel plates separated by the distance from the port to the speed nut periphery ($C_d = \varepsilon A/g$), and by a static cylindrical capacitance [$C_s = 2\pi EL/\ln(L/R\sqrt{3})$] generated by the sensor port hole and the housing and shaft. The fractional change in total effective capacitance, $\Delta C_d/C_s$, was calculated to be less than 1×10^{-4}, which was considered to be too small for accurate measurements.

In a similar analysis, the eddy-current sensor configuration was broken down to dynamic and static mutual inductances resulting in a change in total mutual inductance of less than 2×10^{-5}, once again too small for accurate measurements.

The electromagnetoacoustic sensor, consisting of an eddy-current sensor superimposed with permanent magnets, was determined to be no more sensitive than the eddy-current sensor.

FFT Group Analysis

The feasibility of the fiberoptic proximeter, accelerometer, pressure pulsation, and acoustic speed sensing technologies was evaluated using data available from previous turbopump tests. The data were reprocessed to provide power spectral density (PSD) plots, time profiles, and isoplots, with the goal of identifying shaft speed related signals valid over the 500 to 50,000 rpm range of the turbopump. In all cases, the data indicated the presence of intermittent and unreliable signals below at least 3000 rpm, rendering these approaches unacceptable to meet the SSME requirements.

The fiberoptic proximeter data revealed numerous bearing-related signals. The shaft rotation/inner race frequency, the cage frequency, the ball pass frequency, and their harmonics were identified in the bearing data. Although strong frequency trends do stand out in the data, there are many periods when the signals are ambiguous and fade out completely, or are superimposed, thus making identification of the frequency component source questionable. It was concluded that there were no readily identifiable amplitude or frequency relationships present that could be counted upon for continuous speed measurement over the duration of the tests.

The analyses of accelerometer data from previous SSME high pressure oxidizer turbopump tests has yielded readily identifiable synchronous frequencies and impeller blade-wake frequency harmonics (4x and 8x synchronous frequency) at

steady-state high rpm speeds. However, the high pressure oxidizer turbopump data often contained High Pressure Fuel Turbopump (HPFTP) vibration signals, and all of the high pressure oxidizer turbopump related signals were found to have periods of intermittence during the tests. For example, no speed-related signals were found below 13,200 rpm and all synchronous frequencies below 3000 rpm were masked by noise.

Pressure pulses obtained from the SSME high pressure oxidizer turbopump high-frequency pressure sensors were responsive to changes in portions of turbopump speed ramp down (from 27,600 to 19,500 rpm) and ramp up (higher than 25,000 rpm) beyond 3 seconds after startup. The lack of reliable speed-linked pressure pulsations during all other turbopump operating conditions renders this technology unsuitable for closed-loop speed measurement over the required rpm range.

The ultrasonic vibration measurement system reported by Hamilton (cited in the Bibliography) presented test results of a small (1/4-inch diameter shaft) universal motor, but did not include any power spectral density curves of the output signal. It is our opinion that such an analysis would have produced power spectral density plots similar to the ones obtained from fiberoptic deflectometer, accelerometer, and pressure pulsation measurements and followed, therefore, their destiny: the signal would be intermittent, weak, and unreliable at low speeds. Therefore, this acoustic technology was also removed from consideration for experimental evaluation.

Isotope Group Analysis

An analysis was performed to determine the total photon count at the isotope speed sensor detector and the relationship between the isotope source strength and the accuracy of speed measurement. For simplicity, it was assumed that the total photon count is proportional to source strength, solid angle of capture, absorption losses, detector efficiency, rotation period, multiplicity of isotope decay, and viewing angle. Specifically, it was assumed that the

source had 5 millicurie strength, a decay multiplicity of 2, 1.1 MeV energy, a 1 percent solid angle capture, and is placed 2.7 inches away from an 80-percent efficient detector. With the above assumptions, a total photon count of only 2 was calculated at 30,000 rpm, which implies a 70-percent scatter (equivalent to one standard deviation) in measurement.

To approach a $\pm$25 rpm accuracy, 4 million counts are required, indicating that the isotope approach would require an extremely high strength source which would not be NRC-exempt, rendering it impractical.

Magnetic Group Analysis

An analysis was performed to determine the amplitude of the signal generated in a pickup coil by the rotating permanent magnet of the variable-source magnetic speed sensor, as shown in Figure 5. It was assumed that if a peak magnetic induction of 6 Gauss can be generated by each of the four shaft-mounted magnets in a pickup coil at a distance of 2 inches, then the induction at the coil would vary from 0 to 6 Gauss over the time interval required for the shaft to rotate one quarter turn, according to Faraday's Law. The voltage generated at the lowest speed (500 rpm) from a linear magnetic field distribution in an air-core pickup coil having 2400 turns (similar to the existing sensor coil) with a cross section equal to the existing port area was determined to be 4.7 mV, using an analysis based upon Faraday's Law. In practice, the magnetic field does not vary linearly. Rather, a much sharper flux density change over a distance approximately equal to the width of the magnet would be observed.

The analysis of Hall-effect or Wiegand-effect magnetic speed sensors follows the analysis of the variable-source magnetic speed sensor except that in these approaches, the detector is not a pickup coil but is either a Hall-effect or Wiegand-effect detector. Hall-effect detectors require external excitation and so were rejected due to the possible hazard they could pose in a liquid

VARIABLE-SOURCE MAGNETIC SPEED SENSOR

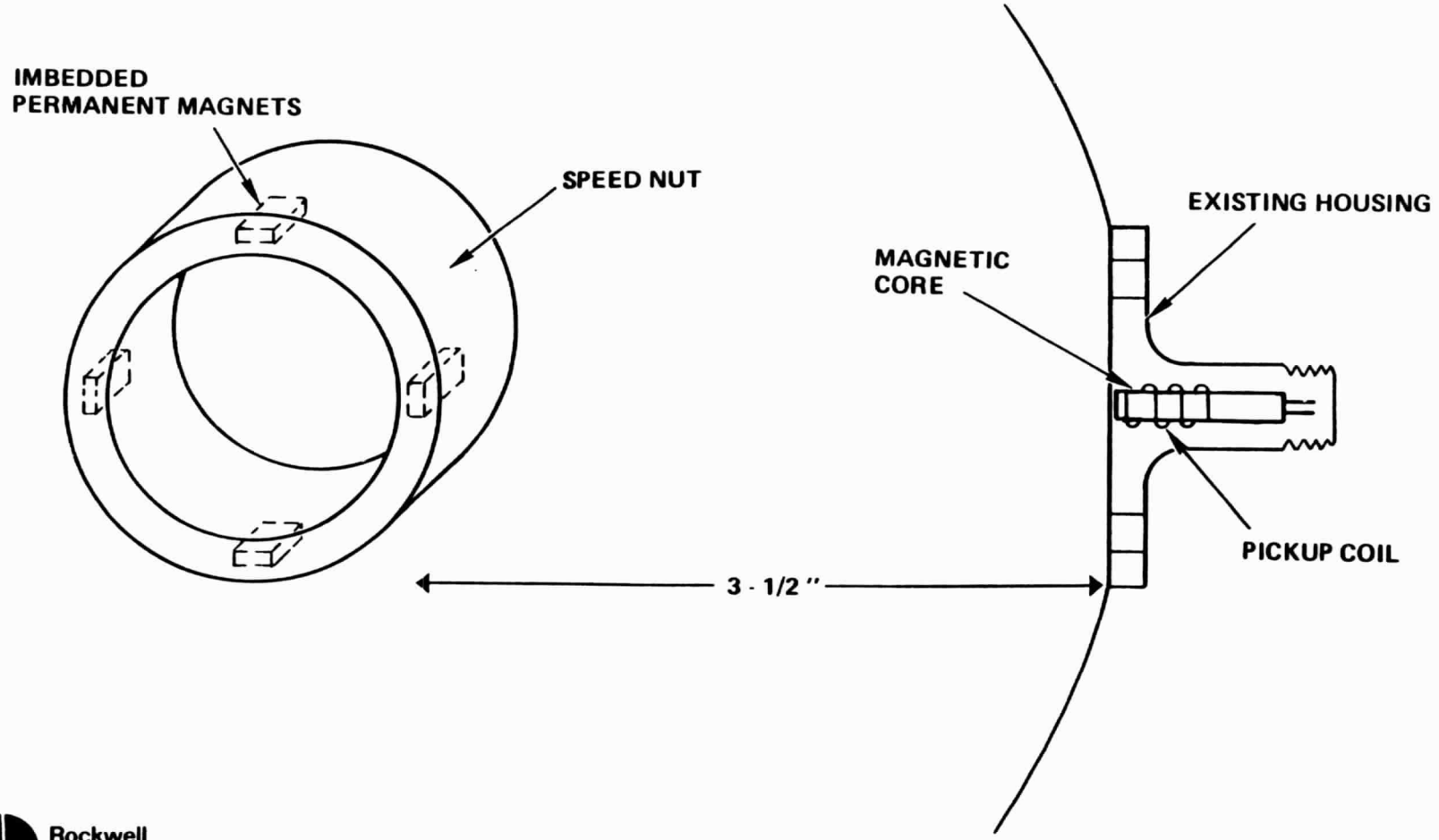

486-120 B

Rockwell International
Rocketdyne Division

Figure 5

oxygen environment. The Wiegand-effect detector generates a constant-amplitude signal due to triggering of a magnetically soft core, but requires impractically high magnetization levels for triggering and was not recommended for experimentation due to the anticipated low levels of magnetization that would be generated in a Wiegand device by permanent magnets 3.5 inches away.

Electromagnetic Group Analysis

Both the microwave and the infrared approach to non-intrusive speed sensing must demonstrate sufficient immunity to propellant cavitation to be considered as viable technologies. An analysis was therefore performed to determine the impact of cavitation on the effectiveness of these techniques.

From the Mie theory, the transmittance, T, through a medium with non-absorbing spherical scatterers takes the form:

$$T = \exp(-N\pi R^2 QL) = \exp(-3CQL/4R)$$

where N = bubble concentration (cm^{-3}) = $3C/4\pi R^3$

C = cavitation fraction (by volume)

R = bubble radius (cm)

L = path length (20 cm roundtrip)

Q = scattering coefficient = $2-(4 \sin P)/P + 4(1-\cos P)/P^2$

$P = 4\pi R(1-M)/\lambda$

M = ratio of refractive indices ($n_1/n_2 = 0.8$)

λ = wavelength (cm)

Transmittances were calculated for assumed levels of cavitation (0.1 and 1 percent) for visible, infrared, and microwave wavelengths for bubble radii on the order of the wavelength utilized and for bubble radii much larger than the wavelength. The results of the calculations are presented in Table 3. For bubble sizes approximately equal to the wavelength the transmittances for both

TABLE 3

MIE SCATTERING TRANSMITTANCE

FOR BUBBLE RADII ≈ WAVELENGTH:

ENERGY FORM	WAVELENGTH	TRANSMITTANCE	
		0.001 CAVITATION	0.01 CAVITATION
MICROWAVE	1 CM 0.1 CM	> 0.85 > 0.20	> 0.20 > 10^{-7}
INFRARED	1.29 MICRON 0.847 MICRON	0 0	0 0
VISIBLE	0.6328 MICRON	0	0

FOR BUBBLE RADII FROM 0.01 - 0.5 CM:

ENERGY FORM	WAVELENGTH	TRANSMITTANCE	
		0.001 CAVITATION	0.01 CAVITATION
MICROWAVE	1 CM 0.1 CM	> 0.85 > 0.20	> 0.20 > 10^{-7}
INFRARED	1.29 MICRON 0.847 MICRON	> 0.60 > 0.60	> 0.40 > 0.40
VISIBLE	0.6328 MICRON	> 0.60	> 0.40

0.1 and 1.0 cm wavelength microwaves indicate that acceptable signal levels will be detected even under conditions of severe cavitation, making the microwave approach very promising. The shorter wavelengths, however, suffer considerably from the scattering effects of oxygen bubbles in liquid oxygen. The visible wavelength (0.6328 micrometer) and the shorter infrared wavelengths (0.847 and 1.29 micrometers) undergo severe signal loss by scattering and are rendered unusable. Mie scattering calculations performed at the same cavitation levels, but for bubble radii in the range of 0.01 to 0.5 centimeter demonstrate sufficient transmittance (greater than 40 percent) for both the infrared and microwave approaches to be usable for remote speed sensing applications.

It is prudent to understand the assumptions inherent in the scattering derivation. It is assumed that all scattered light, including that scattered at small angles, is considered to be removed from the beam. This is equivalent to saying that the detector is assumed to be a very large distance from the scatterer, thus subtending an infinitesimally small solid angle. However, a practical application of microwave and infrared speed-sensing technologies will employ detectors at finite distances, thus subtending finite solid angles. Studies of the angular distribution of scattering indicate that a large portion of the scattering occurs in the forward direction (i.e., toward the detector), suggesting that the effective throughput will be much greater than that indicated by the tabulated Mie scattering results.

Recommendations

The analysis of the 14 candidate technologies has screened from consideration (1) those approaches that fail to provide acceptable output signal level or accuracy, (2) those with intermittent or otherwise unreliable signals, and (3) those whose performance is masked by the extreme environments present in the SSME. The magnetic, microwave, and infrared technologies demonstrated promise for use in non-intrusive speed sensing and were recommended for experimental evaluation. Specifically, the quantification of signal amplitude of the

variable-source magnetic speed sensor at low rpm and the attenuation of microwave and infrared energy through a cavitating medium were recommended for experimental evaluation to verify the feasibility of these technologies.

TASK III - EXPERIMENTAL EVALUATION

Variable-Source Magnetic Speed Sensor Experimentation

The variable-source magnetic speed sensor was tested in the laboratory to determine the detectability of the signal at low speeds and large separations. Four 0.5-inch diameter, disk-shaped ferrite magnets with measured pole strengths ranging from 400 to 500 Gauss were epoxied to a non-magnetic wheel having an outside diameter equal to the SSME speed nut diameter (see Figure 3). The wheel was rotated with an electric motor at speeds of 240, 480, and 720 rpm and magnetic pulses were observed at various distances from the wheel with an SSME high pressure oxidizer turbopump speed sensor (Figure 6). The results of these tests are graphed in Figure 7, indicating the generation of a useful signal of 0.6 mV_{p-p} at the lowest speed (480 rpm) with a 3-inch separation.

A similar test with a samarium-cobalt magnet having a pole strength of 2000 Gauss produced a signal of 2.4 mV_{p-p} with the existing SSME speed sensor at a distance of 2 inches and a speed of 240 rpm. This was a threefold improvement over the signal derived from the ferrite magnet (0.8 mV at 2-inch separation). Further signal enhancement was obtained by using a pickup coil of larger cross-sectional area (7/8 x 7/8 inch) made from 1000 turns of 38-gage wire. At a distance of 3.5 inches, with an air core and samarium-cobalt magnets at 600 rpm, the hand-made 1000-turn pickup coil provided a 6 mV_{p-p} signal. The signal was then enhanced by the addition of hydrogen-annealed HY-MU-80 cores, resulting in a 19 mV_{p-p} (or 9.5 mV) signal, as shown in Figure 8. It is seen that to increase the signal amplitude from 9.5 mV to the specified 75 mV, only a 7.9 times improvement is necessary. This can readily be achieved by increasing the number of turns,

LOW SPEED MAGNETIC EXPERIMENTATION

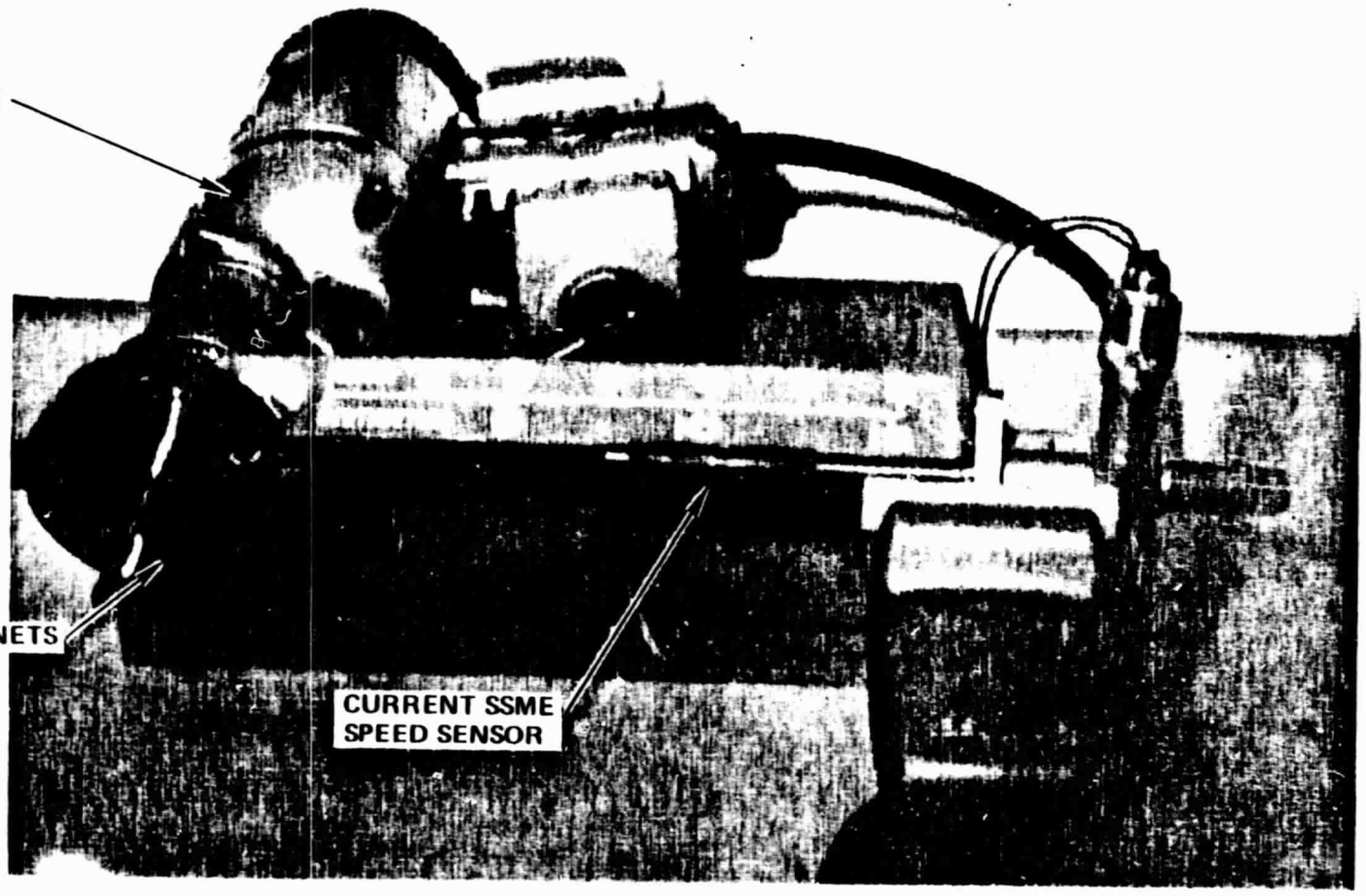

489-455

Rockwell International
Rocketdyne Division

Figure 6

VARIABLE-SOURCE MAGNETIC SPEED SENSOR

(ELECTRICAL SIGNAL AND FIELD STRENGTHS VS SEPARATION OF MAGNET FROM COIL)

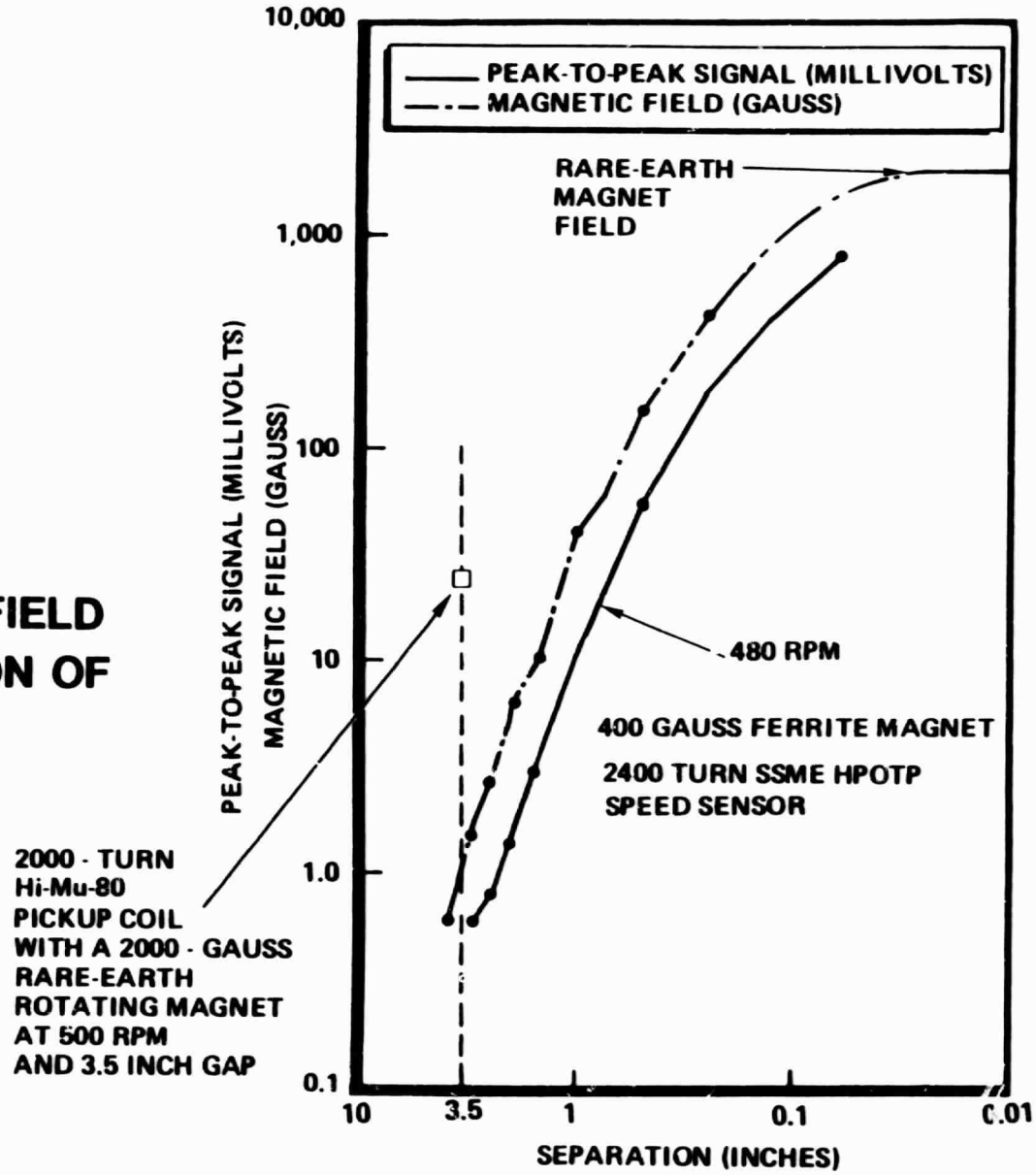

487-709

Rockwell International
Rocketdyne Division

Figure 7

VARIABLE-SOURCE MAGNETIC SPEED SENSOR OUTPUT

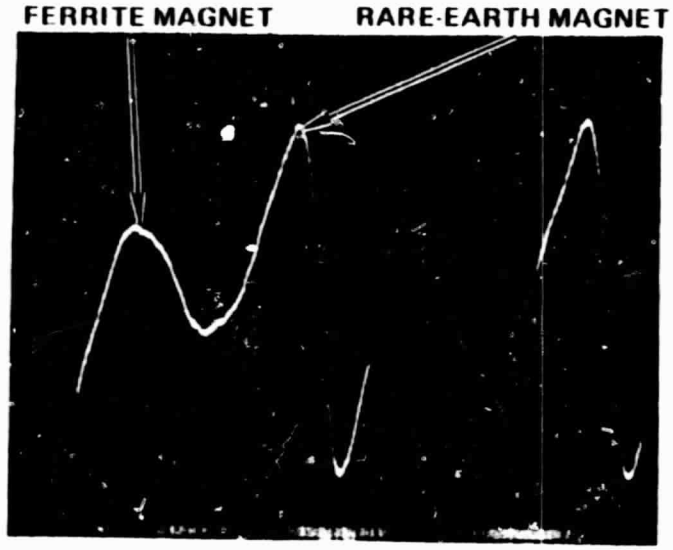

(a) AIR CORE

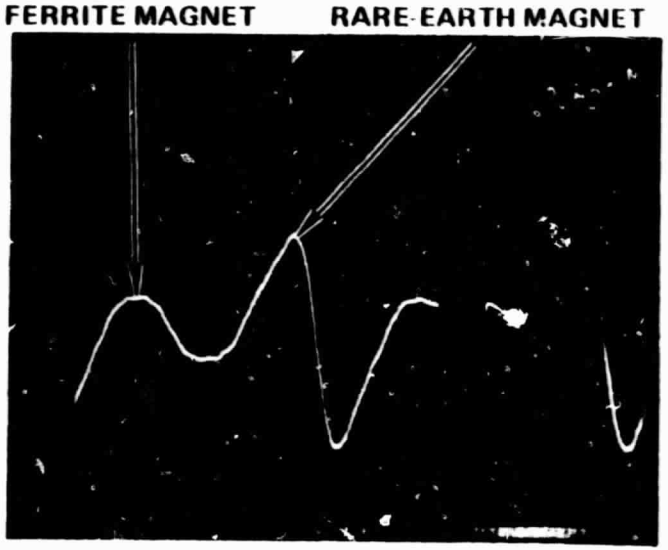

(b) HY-MU-80 CORE

489-456

Rockwell International
Rocketdyne Division

Figure 8

the length of core, the area of the coil, the magnetic field gradient, the permeability of the core, or by decreasing the gap. Another approach is to benefit from a combination of all the above-mentioned parameters.

Additional tests were performed at higher rpm's to determine the high-frequency shielding effect of turbine vanes and housing placed between the coil and magnets, as shown in Figure 9. Four ferrite magnets were next molded into an epoxy ring on a 2-inch diameter aluminum tube, which was spun over a speed range of 2000 to 6000 rpm with an existing test rig. Output pulses from a 2000-turn (7/8 x 7/8 inch) air core pickup coil were measured at a distance of 3.5 inches from the magnets, as shown in Figure 10. Various metal plates were held tightly against the nylon spool of the pickup coil, simulating a housing-mounted coil as shown in Figure 5. The results of the shielding of these plates are also shown in Figure 10, where a 1.2 x 12 x 18 inch Inconel 718 plate and 1.75 x 12 x 12 inch Inconel 625 plate did not attenuate the signal at all, yet a 0.75 x 7 x 16 inch aluminum plate significantly reduced the signal.

The cause of this difference in signal reduction between aluminum and Inconel is due to the difference in electrical resistivity of the two metals. Aluminum is a very good conductor whose resistivity ranges from 1 to 3 microhm inches depending on the temperature, heat treatment, and alloy composition. The resistivity of Inconel is substantially greater than that of aluminum and ranges from 39 to 48 microhm inches even at cryogenic temperatures. Thus, eddy currents are not readily set up in Inconel, and the original magnetic field is not cancelled by its passage through Inconel.

A Hall-effect Gaussmeter was used to investigate the characteristics of the instantaneous rotating magnetic field. The Gaussmeter probe was placed 0.4 inch from four rotating ferrite magnets. Figure 11 shows the positive and negative distinct magnetic field spikes associated with the four alternately-polarized ferrite disc magnets. At speeds varied from 0 to 2400 rpm, the Gaussmeter provided a constant-amplitude signal, tapering down at the

VARIABLE-SOURCE MAGNETIC SPEED SENSOR EXPERIMENTAL SETUP

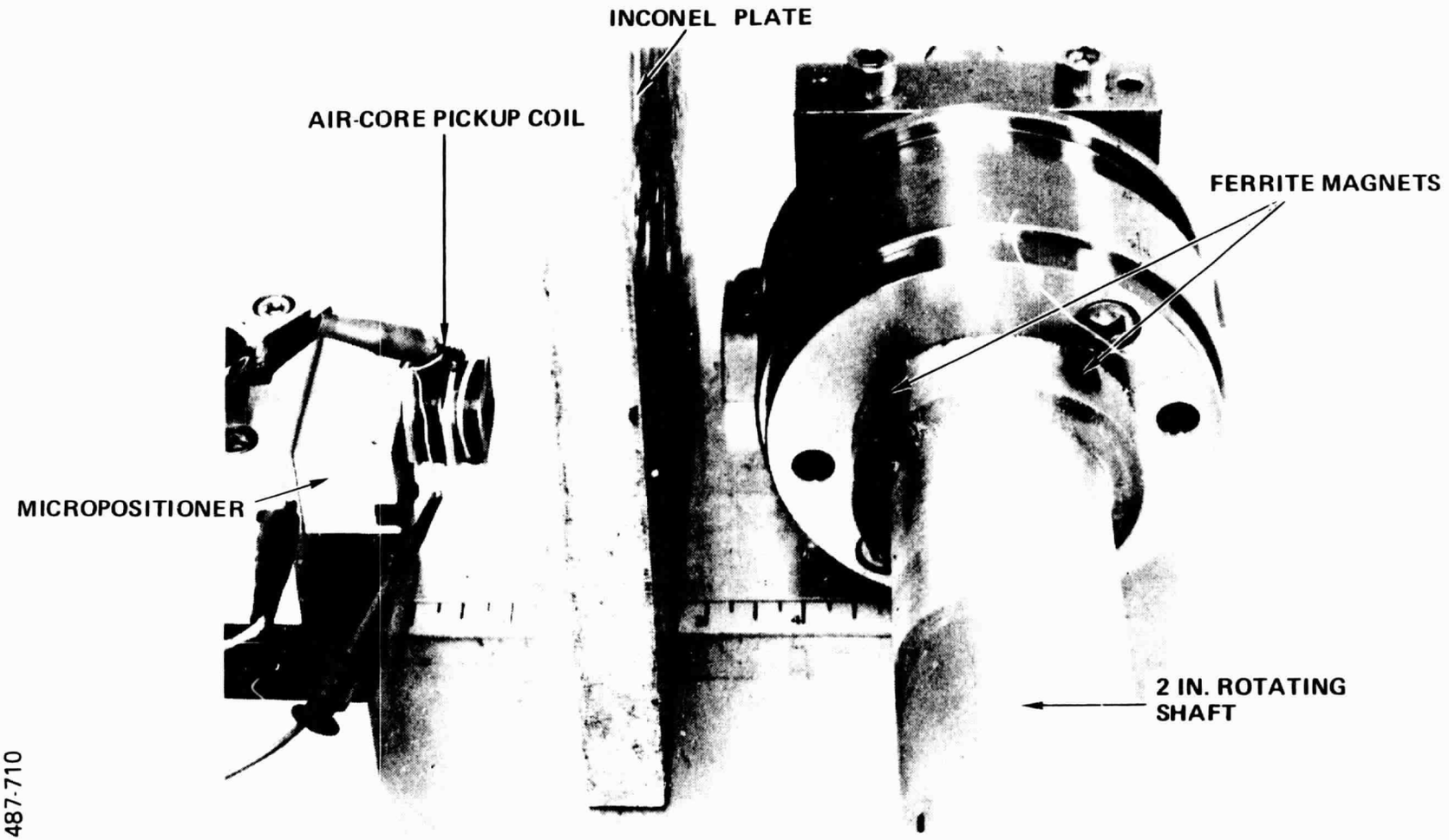

487-710

Rockwell International
Rocketdyne Division

Figure 9

VARIABLE-SOURCE MAGNETIC SPEED SENSOR

SIGNAL AMPLITUDE VS ROTATING SPEED

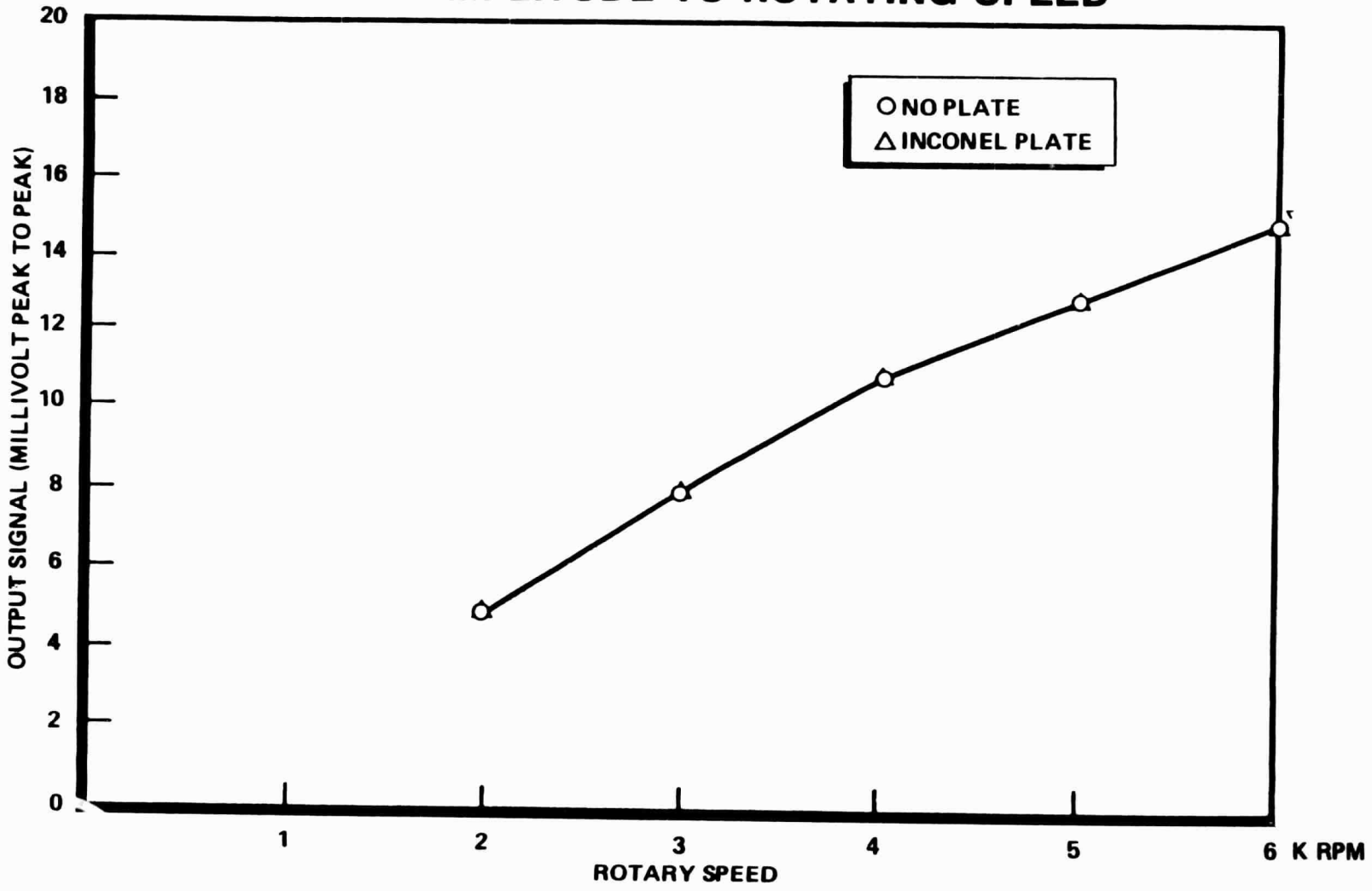

487-711

Rockwell International
Rocketdyne Division

Figure 10

HALL PROBE OUTPUT

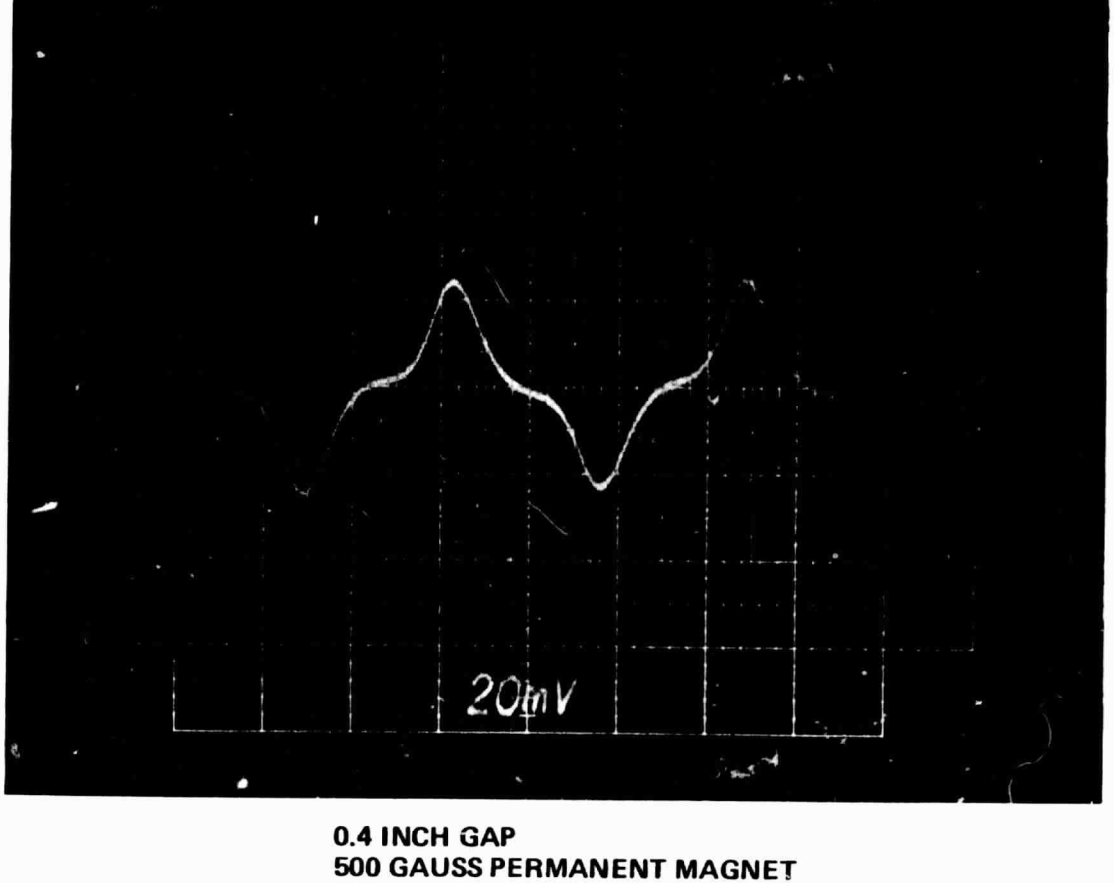

0.4 INCH GAP
500 GAUSS PERMANENT MAGNET
400 HZ HALL PROBE
2400 RPM

488-597

Rockwell International
Rocketdyne Division

Figure 11

higher shaft speeds as the 400-Hz Gaussmeter frequency response attenuated the transients (Figure 12).

It is seen that the Hall-effect probe provides a nearly constant-amplitude signal independent of shaft speed. This is because it measures the instantaneous amplitude of magnetic field. In contrast, pickup coils measure the time rate of change of the magnetic field, which is linearly dependent on shaft speed. Further more, the pickup coil acts as a low-pass filter, thus reducing the effective signal amplitude because of the high-frequency nature of the individual spikes. In conclusion, it was learned that the Hall-effect probe can generate larger output signals than a pickup coil under the same conditions.

In summary, the variable-source magnetic speed sensor, even at low speeds, can generate strong signals at a 3.5-inch distance from the speed nut, and does not lose any signal due to eddy currents in the existing intervening turbopump housing or vane materials. Thus, this sensor can be mounted completely externally on the turbopump housing. In view of this non-intrusiveness, and of the sensor's use of space-proven hardware and its inherent immunity to bubbles and cavitation, we conclude that it is a highly viable and desirable sensor for the SSME.

Infrared Cavitation Experimentation

The infrared cavitation experiment required the use of a bubbler apparatus, test chamber, light source, and a detector, as shown schematically in Figure 13. The hardware was arranged in a closed-loop system which recirculated distilled water into which air was injected through a 40-60 micrometer filter. Figure 14 shows the operational layout of the hardware and demonstrates the c ear, bubble-free liquid entering the bottom of the gas injector and the white, foamy, liquid exiting at the top of the test chamber. The laser directed its beam through a zinc selenide window (transparent from the visible to beyond 20 microns) into the cavitated medium, out of another

HALL PROBE RESPONSE

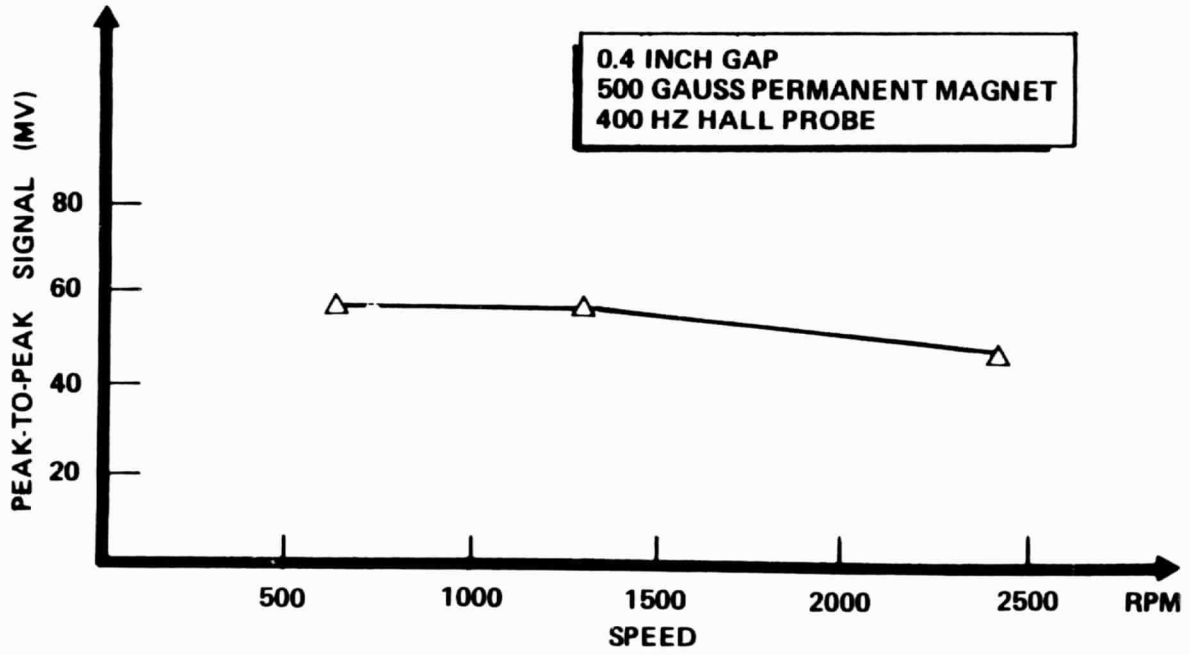

488-585

Rockwell International
Rocketdyne Division

Figure 12

INFRARED CAVITATION EXPERIMENTATION LAYOUT

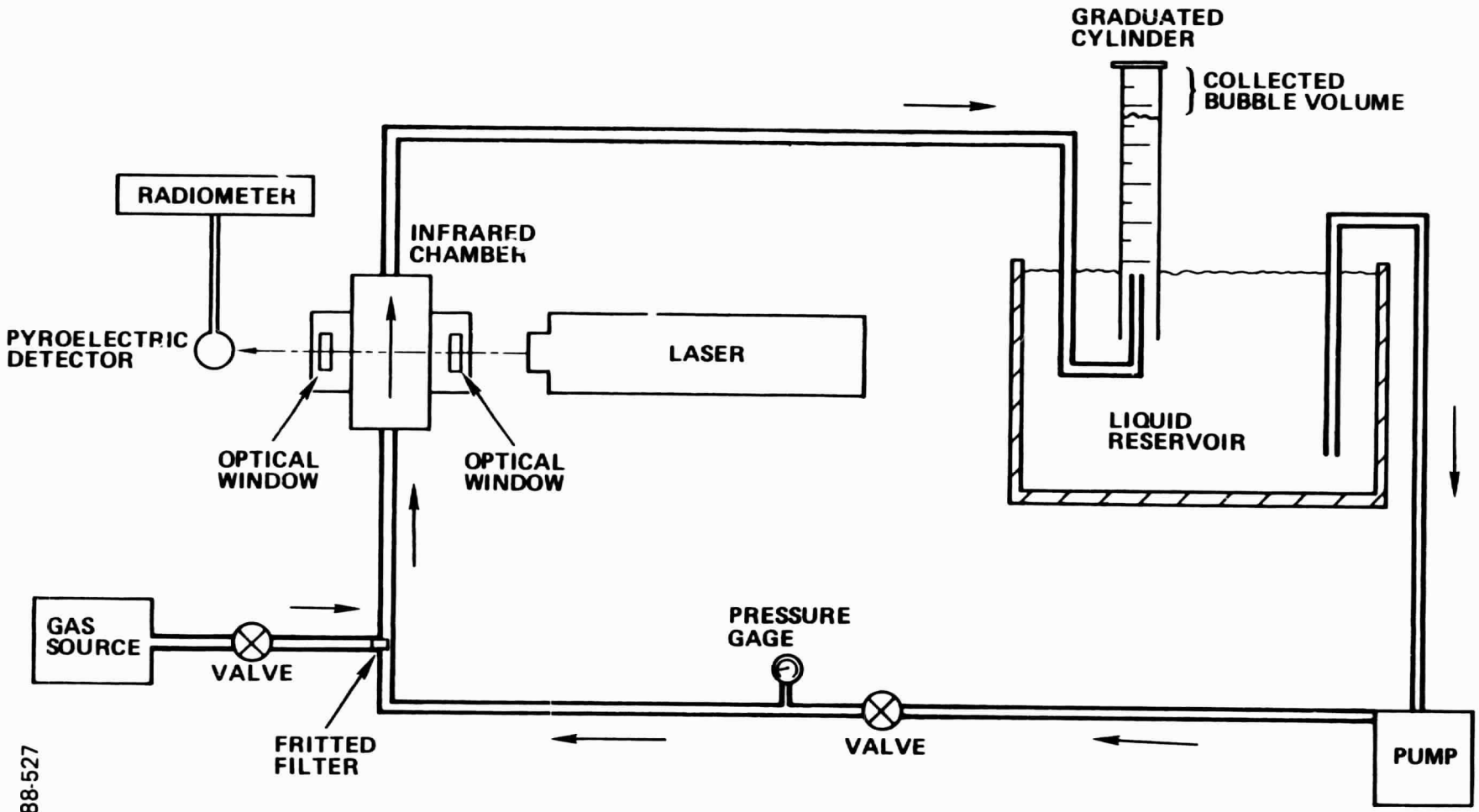

Figure 13

INFRARED EXPERIMENTATION HARDWARE

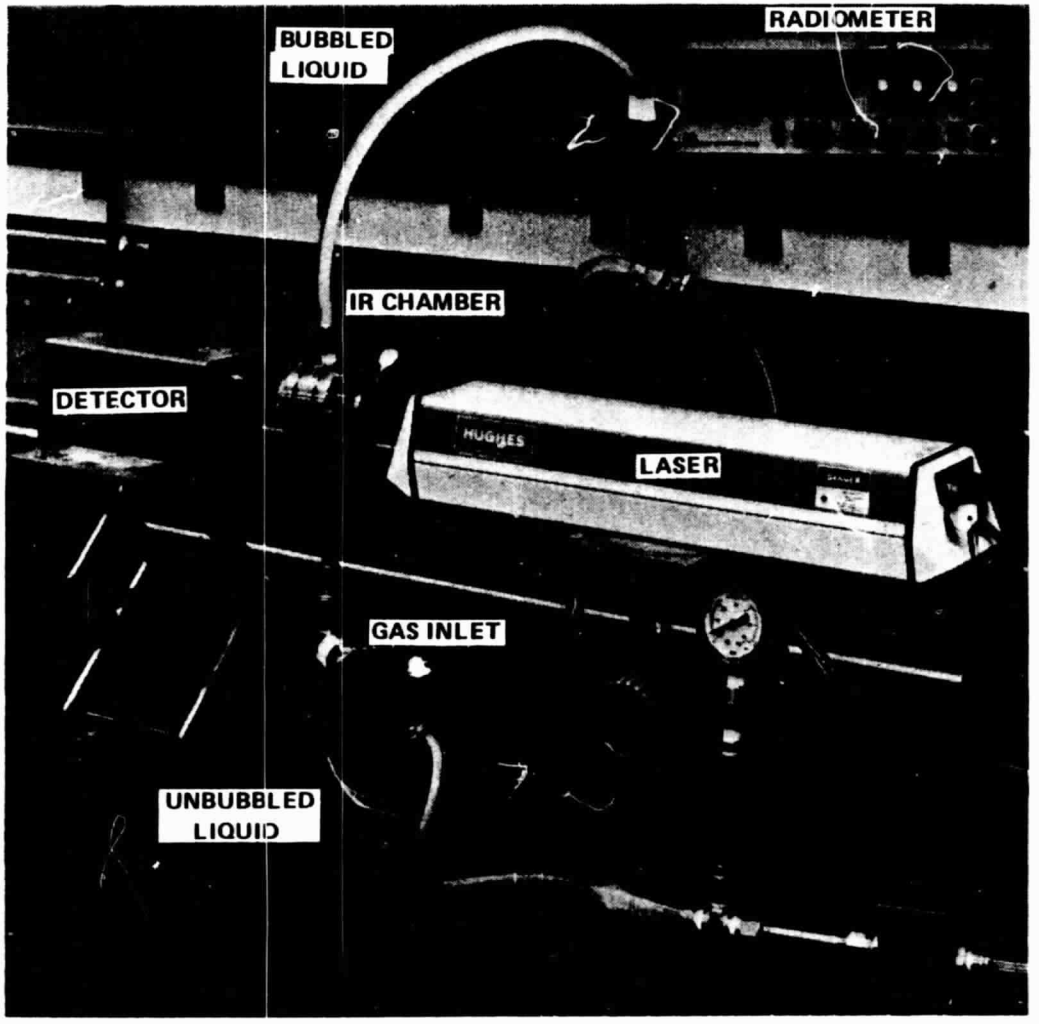

488-615

Rockwell International
Rocketdyne Division

Figure 14

zinc selenide window, and into the broadband (visible to far infrared) pyroelectric radiometer detector head. The detector output was read on the radiometer panel, as shown at the upper right of the photograph. Figure 15 shows the pump used to recirculate the liquid medium, and the inverted graduated cylinder which collects the previously injected gas to determine the cavitation fraction of the bubbled liquid.

During a given run of the cavitation experiment, a laser power level baseline was first established by beaming the laser directly onto the 0.1 cm^2 pyroelectric detector element and recording the laser output power. The infrared chamber was next inserted into the beam so that the beam traversed the optical centerline of the chamber, and the system was once again aligned to maximize the output signal and establish the chamber/unbubbled liquid throughput power level. Once this was recorded, the liquid pump was turned on and the flow rate was measured by dividing the volume of the liquid accumulated by the collection time. Next, the signal level was allowed to stabilize (nominally at about 99% of the previous reading). From this point, gas was injected at a very slow rate and, after signal stabilization, the power level was recorded every 30 seconds over a 3 minute period, during which time the bubbles were collected in the inverted graduated cylinder. This bubble volume was compared with the predetermined liquid flow volume over the same time period to determine the cavitation fraction (which is equal to bubble volume divided by liquid volume). The gas flow rate was increased and the power level and bubble volume measurements were performed again for a different cavitation fraction.

The experimentation was initially performed at the visible wavelength of 0.6328 micrometer and later extended to an infrared wavelength of 0.847 micrometer. It was determined that the two liquid media (carbon tetrachloride and carbon disulfide) suggested for use with the longer wavelengths, would require definitive safety practices to prevent the exposure of laboratory personnel to these liquids and their vapors. Such precautions were significantly beyond the scope of the experimentation so as to render these liquids impractical for use.

RECIRCULATING PUMP AND GAS COLLECTION APPARATUS

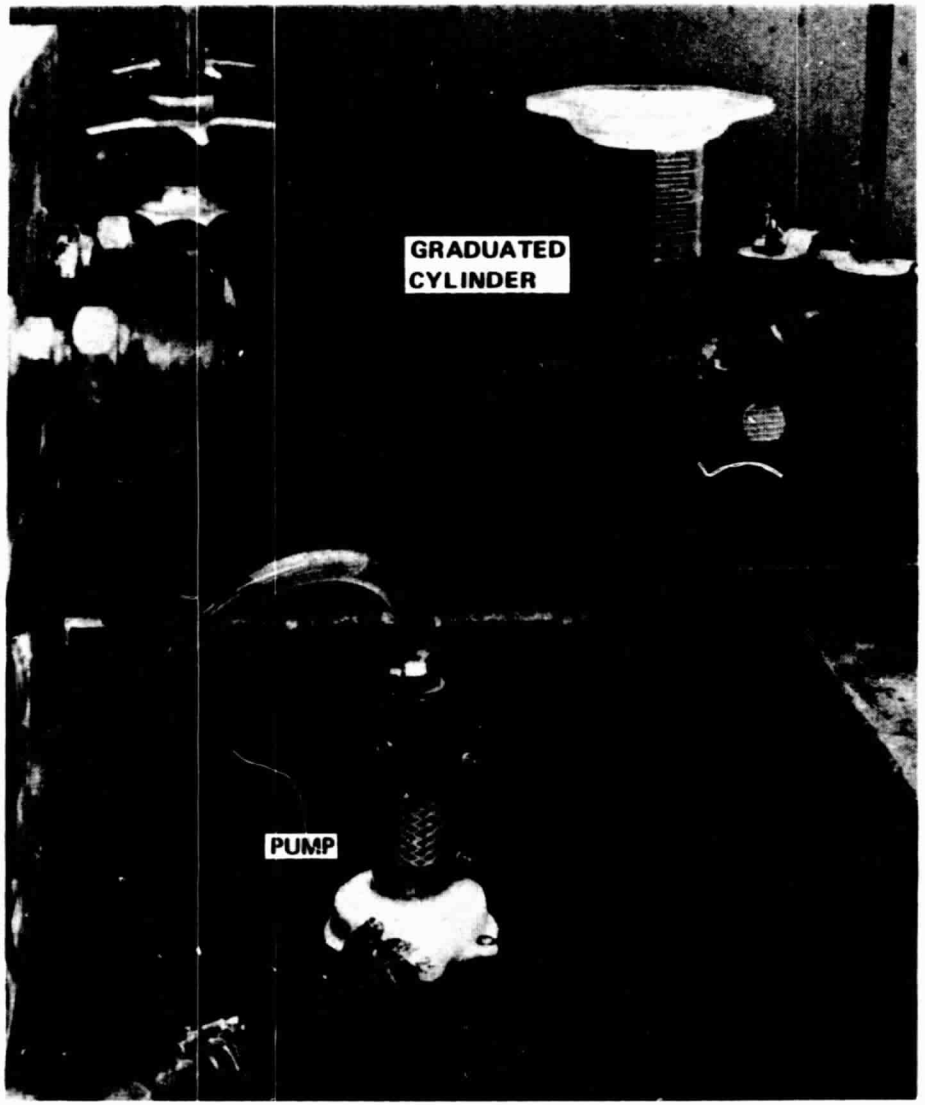

488-614

Rockwell International
Rocketdyne Division

Figure 15

An attempt was made to use the 3.39 micrometer wavelength light with water, but no usable signal could pass through the water in the chamber, as suggested by the absorptance spectra of water. An additional experiment was performed with an incandescent light source filtered to provide only 1.29 micrometer light. Once again the absorption coefficient of water reduced the throughput to well below the detection level of the radiometer.

Observations of the bubbles flowing through the chamber have shown the bubble radii to range from 0.01 centimeter on up to about 0.5 centimeter. The experimental data from the infrared cavitation experiment is shown in Figure 16. These experimental results show a larger throughput than that calculated by theory, and can be understood from the assumption inherent in the scattering calculations that all light, no matter how slightly scattered, is removed from the beam. In most practical applications there is a finite-sized detector close to the liquid medium, and this sensor will catch a great deal of the forward-scattered energy, as has probably occurred in these experiments.

It is important to note that the wavelengths involved in this experiment, 0.6328 and 0.847 micrometers, are both much smaller than the range of observed bubble sizes (100 to 5000 micrometers), and are similarly governed by geometrical optics considerations, thus accounting for the similar experimental results for the two wavelengths. The plotted Mie scattering calculations are the same for both wavelengths.

Microwave Cavitation Experimentation

The microwave cavitation experiment required the use of a bubbler apparatus, test chamber, microwave energy source, and a detector, as shown schematically in Figure 17. The hardware was arranged in a closed-loop system which recirculates liquid nonane into which gaseous nitrogen was injected. The bubbler apparatus used for the microwave experimentation was the same as that used for the infrared experimentation.

TRANSMITTANCE THROUGH 6.5 cm OF BUBBLED WATER

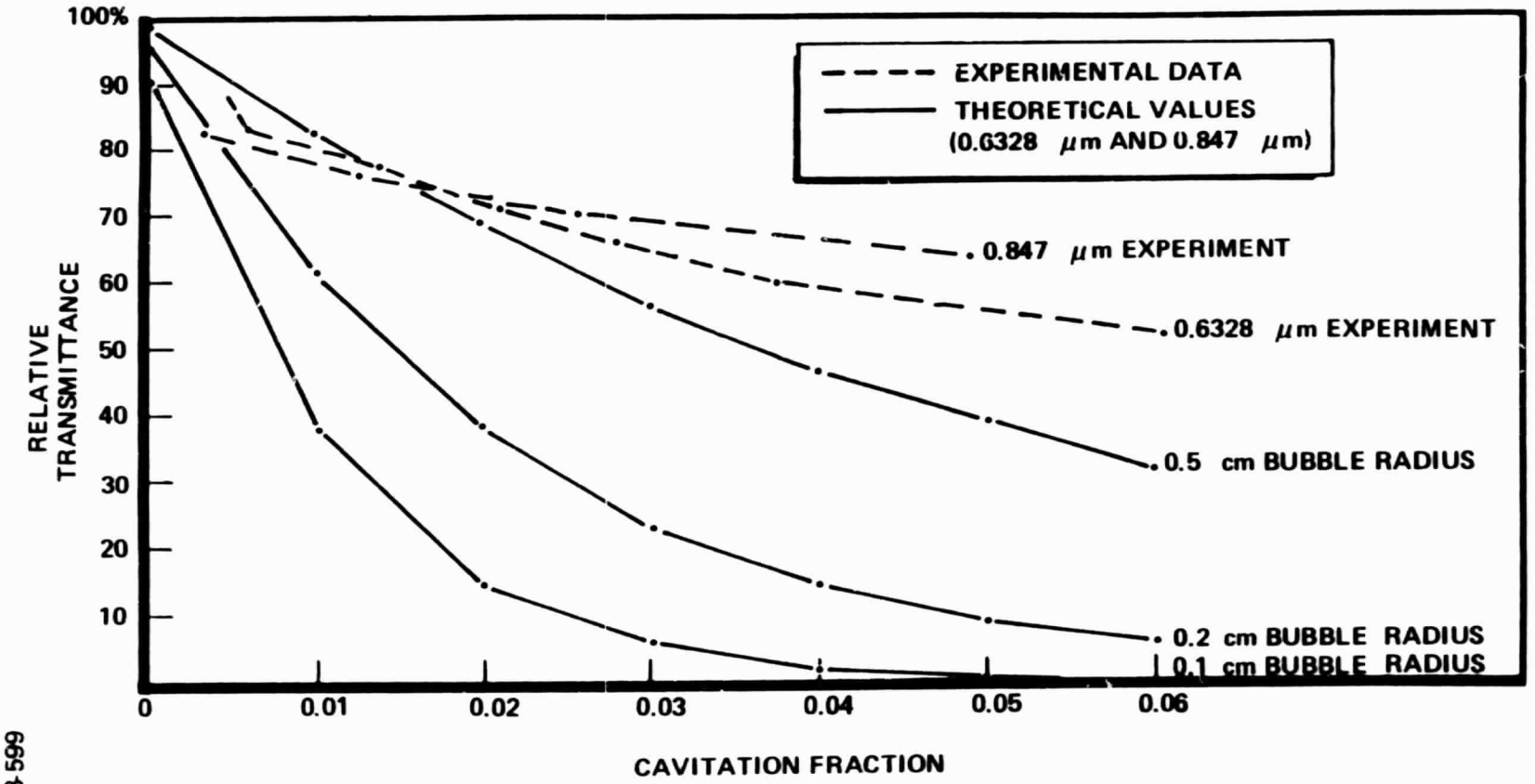

488-599

Rockwell International
Rocketdyne Division

Figure 16

MICROWAVE CAVITATION EXPERIMENT SCHEMATIC

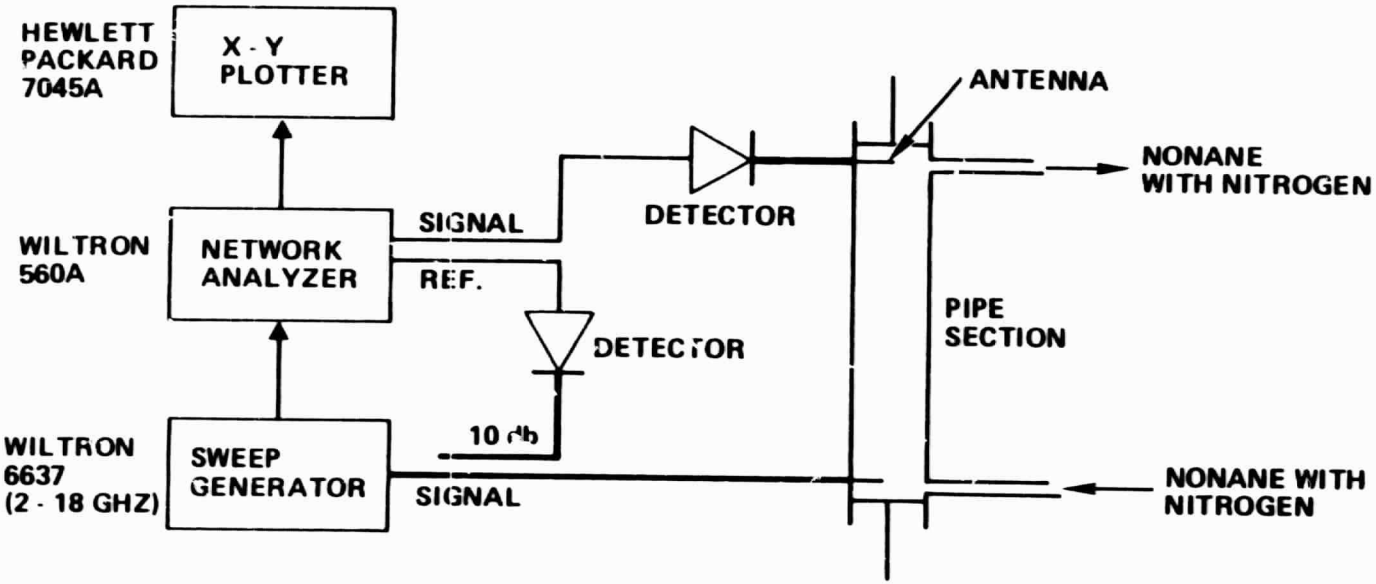

488-622

Rockwell International
Rocketdyne Division

Figure 17

The microwave test chamber, shown in Figure 18, was constructed of AN-pipe hardware with SMA bulkhead fittings installed in each tee. The antennae were constructed by soldering lengths of 20-gauge wire to the interior of the SMA fittings such that the wire extended half-way into the tee cavity. The two antennae were separated by a length of 3/8" inside diameter pipe which represented the present HPOTP speed sensor access port, and the overall separation between antennae was 5.9 inches. At opposite ends of the test chamber were large, flat-bottomed screws which were used as movable shorts in a cylindrical waveguide and adjusted to initially tune the microwave cavity for optimum transmission.

Also inherent in the design of this experiment was the calculation of the dielectric constants of the nitrogen/nonane mixtures. This was determined by means of the equation given by Looyenga (Physica, 12, 257 (1946)):

$$\epsilon^{1/3} = \sum \epsilon_i^{1/3} \phi_i$$

where ϵ = real part of the complex dielectric constant (relative permittivity) of the mixture,

ϵ_i = real part of the complex dielectric constant of the i^{th} component, and

ϕ_i = volume fraction of the i^{th} component

MICROWAVE TEST CHAMBER

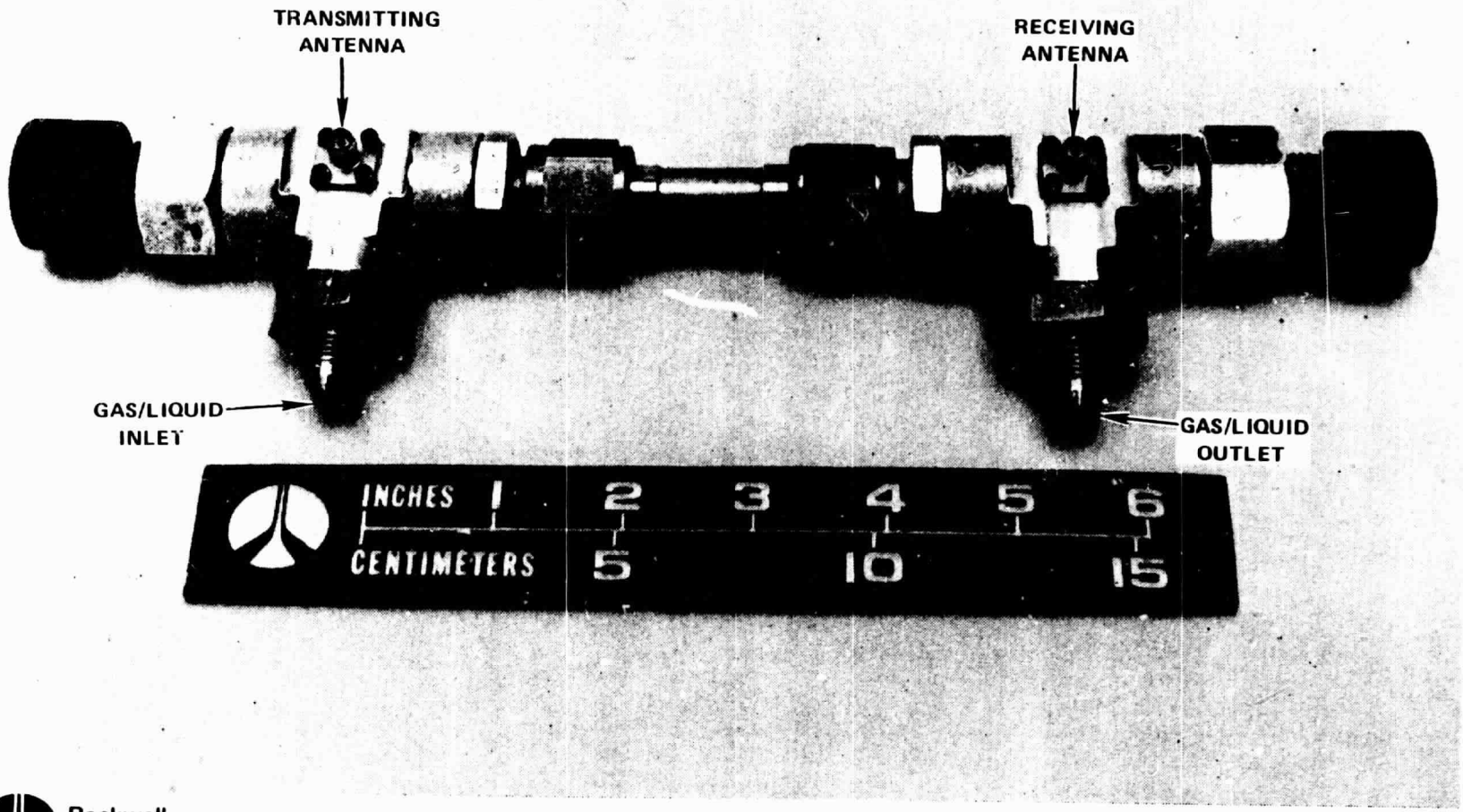

488-613

Rockwell International
Rocketdyne Division

Figure 18

Once the dielectric constant is known, the cut-off frequency of the n,1 mode of propagation ($(f_c)_{TEn,1}$) can be calculated from:

$$(f_c)_{TEn,1} = (K'_c)_{n,1}/2\pi a\epsilon^{-1/2}$$

where $(K'_c)_{n,1}$ = first root of the Bessel function $J'_n(K'_c) = 0$, and

a = radius of the waveguide

This cutoff frequency is the minimum frequency which can propagate in a circular waveguide. The dielectric constants and cutoff frequencies are shown in Table 4 for the cavitation fractions observed during this experimentation.

Static measurements were made with pentane as the unbubbled liquid medium and the test chamber was tuned to accommodate pentane's dielectric constant (ϵ = 1.84) and to provide maximum transmittance at 15 GHz. These preliminary settings provided a good starting point for the nonane experimentation, where the dielectric constant changed from 1.97 to 1.794 as the cavitation fraction increased. It was possible to transmit as much as 5-10% of the microwave energy through unbubbled pentane (as compared with 100% for an air-filled waveguide). Although pentane itself has low absorption characteristics the antennae, with further redesign, could optimize the power throughput substantially. It is important to note that transmittances on the order of 0.01% are sufficient for speed sensing purposes.

Figure 19 and 20 show the relative microwave energy transmittance for various levels of cavitation in nonane. Neither the adjusting screws nor the antennae were precisely optimized at each cavitation level, and the result is a relatively flat transmission curve from 14.7 to 16.5 GHz. Although the maximum transmittance is 0.1 to 0.7%, this could easily be increased by at least a factor of 50 with proper optimization. Even without optimization, these observed transmittances are more than sufficient to provide usable energy throughput.

Table 4

Dielectric Constant and Cut-off Frequencies of N_2/Nonane Mixtures Tested.

Cavitation Fraction	ε	(Fc)TE11 GHz
0.0000	1.97	13.15
0.0149	1.952	13.21
0.0162	1.950	13.22
0.0197	1.947	13.23
0.0360	1.927	13.30
0.1515	1.794	13.78

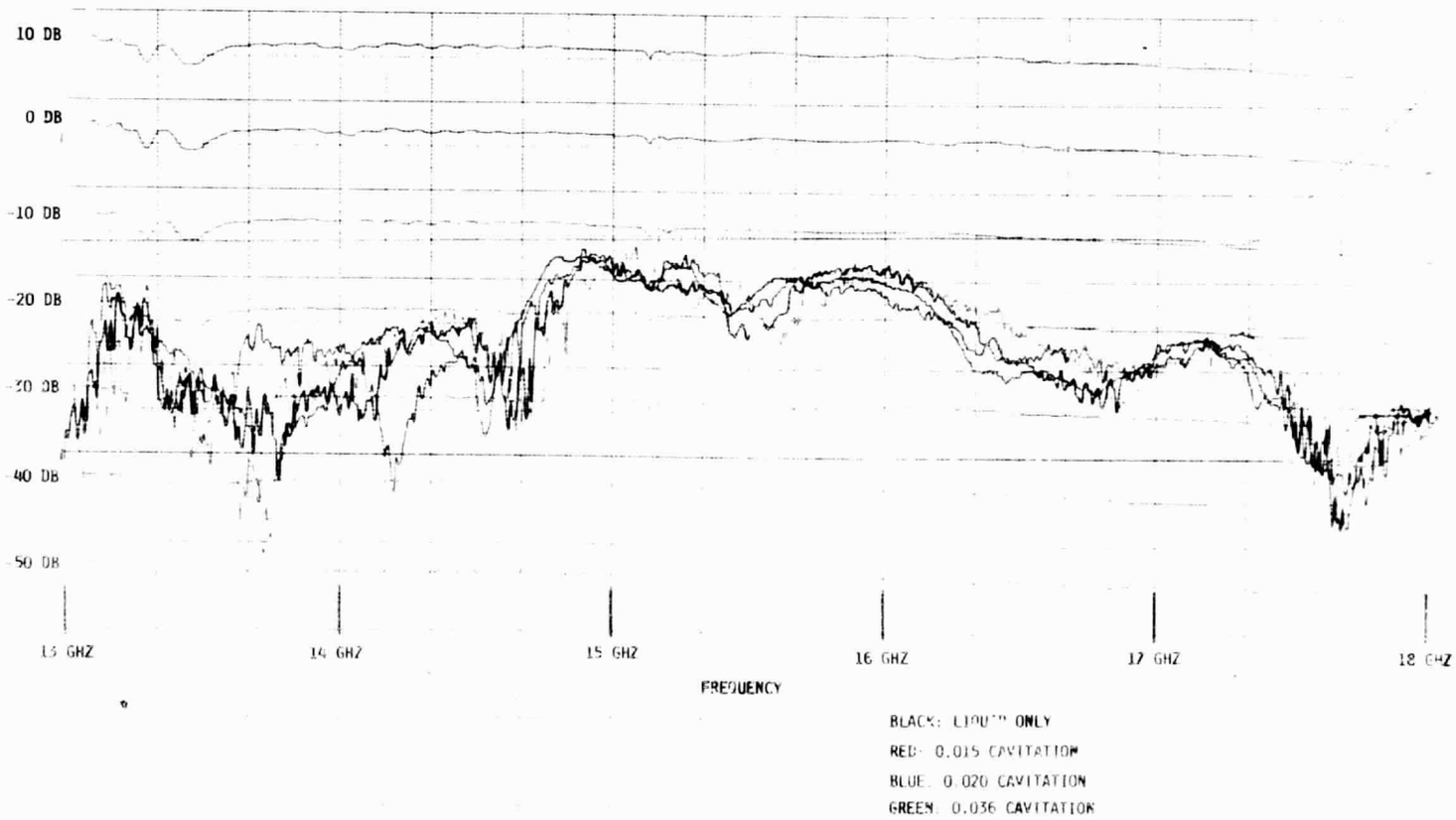

Microwave Transmittance Through Bubbled Nonane

Figure 19

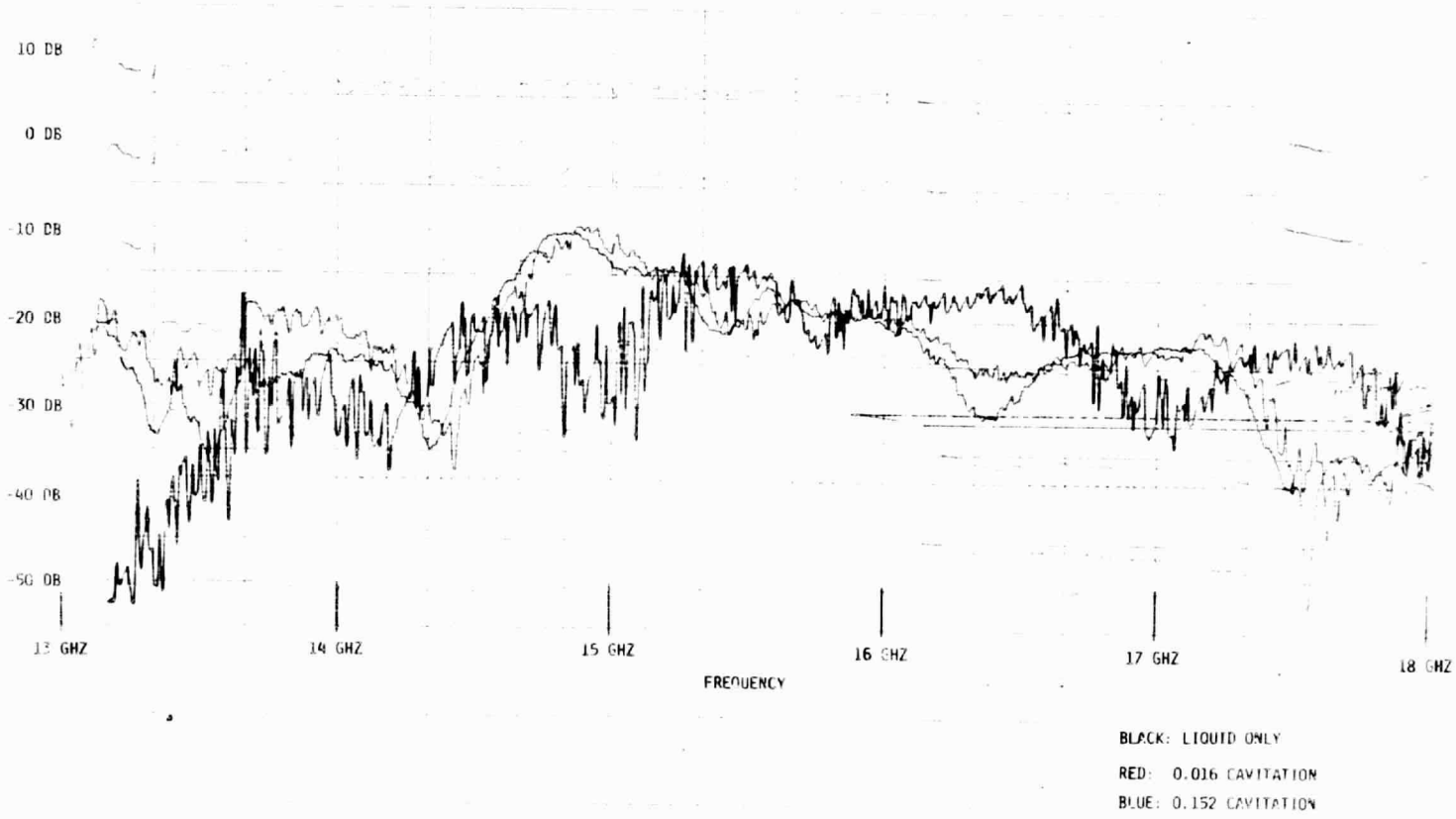

Microwave Transmittance Through Bubbled Nonane

Figure 20

Qualitatively, it can be seen that increased levels of cavitation do not correspond to decreased energy throughput, as can be seen particularly well in several bands in Figure 19. The major effect of increasing the cavitation fraction of gaseous nitrogen in liquid nonane is to shift the cavity resonance mode frequencies, such that the curves overlap and allow each curve to attain a relative maximum over the others at some frequency along the curve. The decrease in transmittance with increased bubble concentration is minimal, consistent with the Mie scattering calculations for these microwave wavelengths (approximately 2 centimeters) interacting with the 0.01-0.5 centimeter radius bubbles produced in these experiments.

It is important to note that the signal is very clean in this frequency range for all but the most extreme cavitation level (15% by volume), where the noise-free signal region has shifted to slightly higher frequencies. At the very high cavitation level shown in Figure 20 there is considerable noise due to the randomness of the instantaneous cavitation fraction. The effluent liquid was not homogeneous due to the large bubbles flowing through the waveguide. The noise level decreases with increasing frequency, suggesting that the high noise is actually variations of the cut-off frequency during the experiment. If this is the case, the higher frequencies (shorter wavelengths) may be more suitable for speed measurement under conditions of extreme cavitation, up until the wavelengths become so short as to be adversely affected by Mie scattering off the bubbles themselves.

The overall results of the microwave cavitation experimentation indicate that the microwave approach shows promise as a non-intrusive speed sensing technology. Although the experiment is not representative of a liquid/gaseous oxygen system at cryogenic temperatures and 5000 psi pressures, the nitrogen/nonane system has a higher dielectric constant than the corresponding oxygen or hydrogen systems. Thus, the data presented here serve as a worst-case measurement of microwave energy transmission through a cavitated medium.

TASK IV - TRADEOFF STUDY

The three successful candidate solutions from the experimental evaluation task must now be fit to the specific problem of providing a viable speed sensor for the HPOTP in the SSME environment. The candidate technology performance ranking was initially planned to evaluate the specified parameters on the basis of percentages of "ideal" specifications, in order to determine an overall figure of merit for each approach. This evaluation procedure is useful in a tradeoff study of a large number of candidates. Since only three technologies remain for consideration after the first three tasks of the contract, it was found to be more useful to perform the tradeoff study in a qualitative manner using their differences rather than their commonality.There were only a few speed sensor requirements which provided a distinction between the three different technologies. These requirements are listed in Table 5.

The need for SSME Controller modification is best avoided by successful candidate approaches. Both the infrared and microwave speed sensors would require electrical excitation from the controller to generate the infrared or microwave signals used in speed sensing, and would require some controller redesign to enable these signal generators. The variable-source magnetic speed sensor, on the other hand, can demonstrate a wire-for-wire compatibility with the existing controller, thus preventing a costly controller redesign effort.

The infrared and microwave components have not, as complete systems, demonstrated their viability in a space environment. Both the magnetic components and the present magnetic speed sensors, however, have a long history of successful in-space operation, and represent no additional risk in the implementation of this new speed sensor.

TABLE 5

TASK IV – TRADEOFF STUDY

FEATURE	MAGNETIC	INFRARED	MICROWAVE
CONTROLLER MODIFICATION	NONE	SLIGHT	SLIGHT
SPACE-PROVEN HARDWARE	YES	NONE	PARTIAL
CONSTANT AMPLITUDE	NO	YES	YES
CAVITATION IMMUNITY	EXCELLENT	LIMITED	GOOD

The infrared and microwave approaches have constant amplitude output signal levels. In contrast, the magnetic approach has an output which is directly proportional to the speed. Although constant-amplitude is desirable, the controller can utilize a varying signal level as long as it remains above the established minimum voltage requirement (75 mV) of the controller at the specified minimum speed (600 rpm). This is demonstrated in the Preliminary Design Task.

The cavitation immunity of present magnetic speed sensors has been well established in the turbopump environment, and is shared by the variable-source magnetic speed sensor. Although, a sufficient degree of cavitation immunity was demonstrated in infrared and microwave cavitation experiments, similar results need to be demonstrated in the operating turbopump environment to show the practicality of these approaches.

Based upon the above assessments, the variable-source magnetic speed sensor emerges as the most attractive approach. Its inherent similarity to the present magnetic speed sensors in terms of controller compatibility, its space-proven hardware, its output signal level, and its cavitation immunity all point toward a very promising approach to HPOTP speed sensing.

TASK V
VARIABLE-SOURCE MAGNETIC SPEED SENSOR PRELIMINARY DESIGN

A preliminary design of the variable-source magnetic speed sensor was performed for the speed nut, probe and electrical components. The design was based upon maximizing the usage of the existing components to minimize turbopump and controller redesign.

From a stress analysis point of view, an open space 0 125" diameter x 0.2" long is available at four positions around the proposed speed nut. These spaces would be filled by samarium-cobalt magnets, as shown in Figure 21.

PROPOSED SPEED NUT

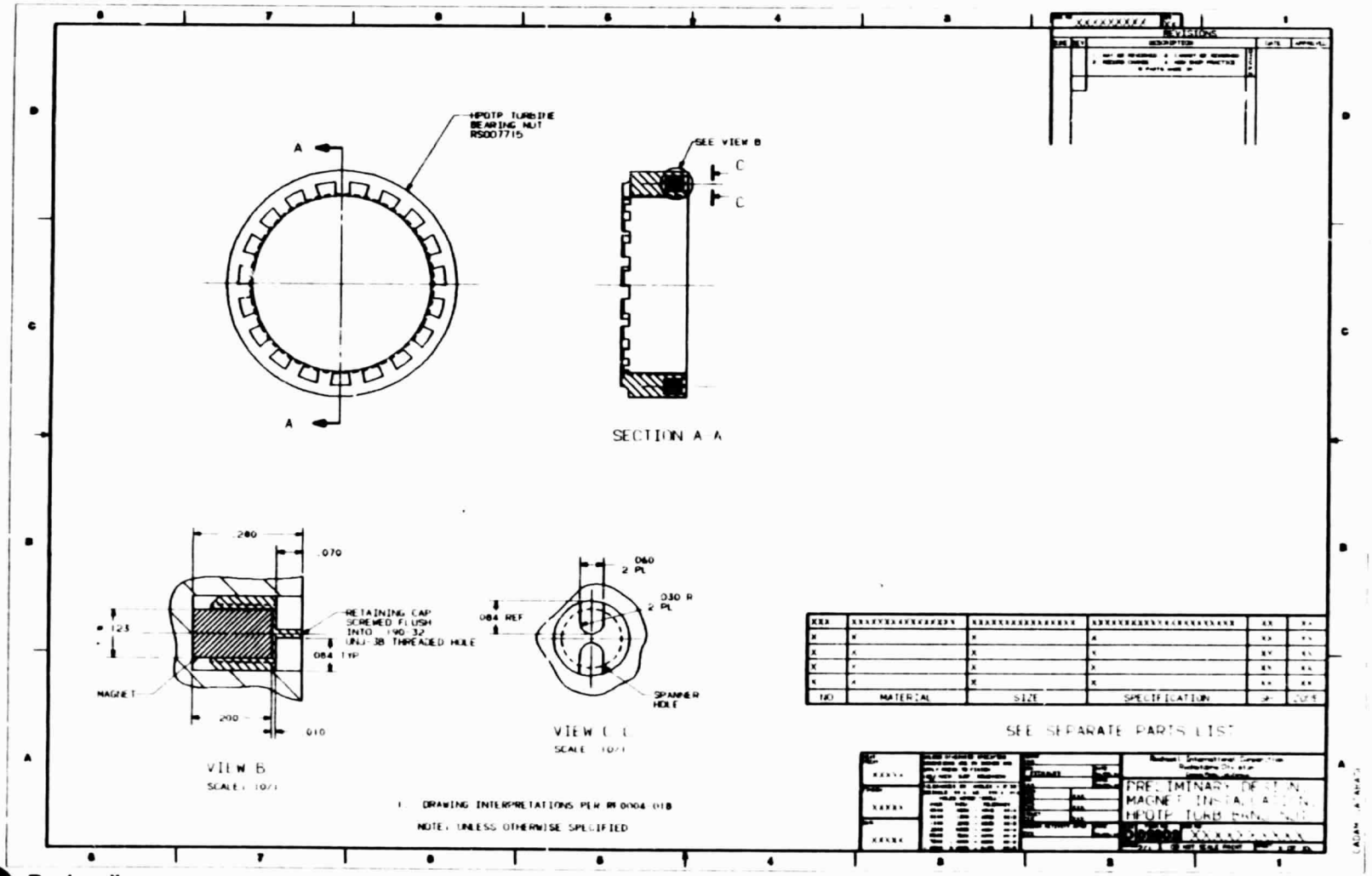

488-530

Rockwell International
Rocketdyne Division

Figure 21

This preliminary magnetic speed sensor probe design utilizes a modified sensor housing from the existing HPOTP speed sensor and places the sensing elements completely outside of the pump as shown in Figure 22. This sensor uses the same mounting holes as the present speed sensor, thus requiring no modification of the HPOTP housing.

The preliminary design of the speed probe electrical components was limited by the controller signal amplitude and frequency response requirements. The speed sensor signal amplitude is proportional to the shaft speed, the number of coil turns, the permeability of the coil core, the area of the coil, and the magnetic field gradient, as indicated by Faraday's Law:

$$V = \mu\omega NA\, \partial B/\partial\theta$$

where

V = output voltage

μ = permeability of core

ω = rotation rate of shaft

N = number of coil turns

A = cross sectional area of coil

$\partial B/\partial\theta$ = magnetic field gradient

We have experimentally observed a 9.5 mV output signal from a 1000-turn coil with a HY-MU-80 core at a distance of 3.5 inches from rare-earth magnets on the surface of a shaft rotating at 600 rpm. This signal can be increased to 75 mV, a factor of 7.9 times improvement, by increasing the number of turns, the length of the core, the coil area, the magnetic field gradient, the core permeability, or by decreasing the gap. The result is shown in Table 6, where all the affected parameters are listed and compared with the existing HPOTP speed sensor specifications. In this Table, the approximate frequency response of a pickup coil represented by an LR circuit was calculated from $f = (R+R_i)/2\pi L$. Assuming a 10 kilohm controller input resistance, a 1530 ohm coil resistance, and a 0.172 Henry coil inductance, a 10600 Hz cutoff frequency is calculated. This value exceeds the 3000 Hz of the RC7005 specification.

PROPOSED SPEED SENSOR PROBE

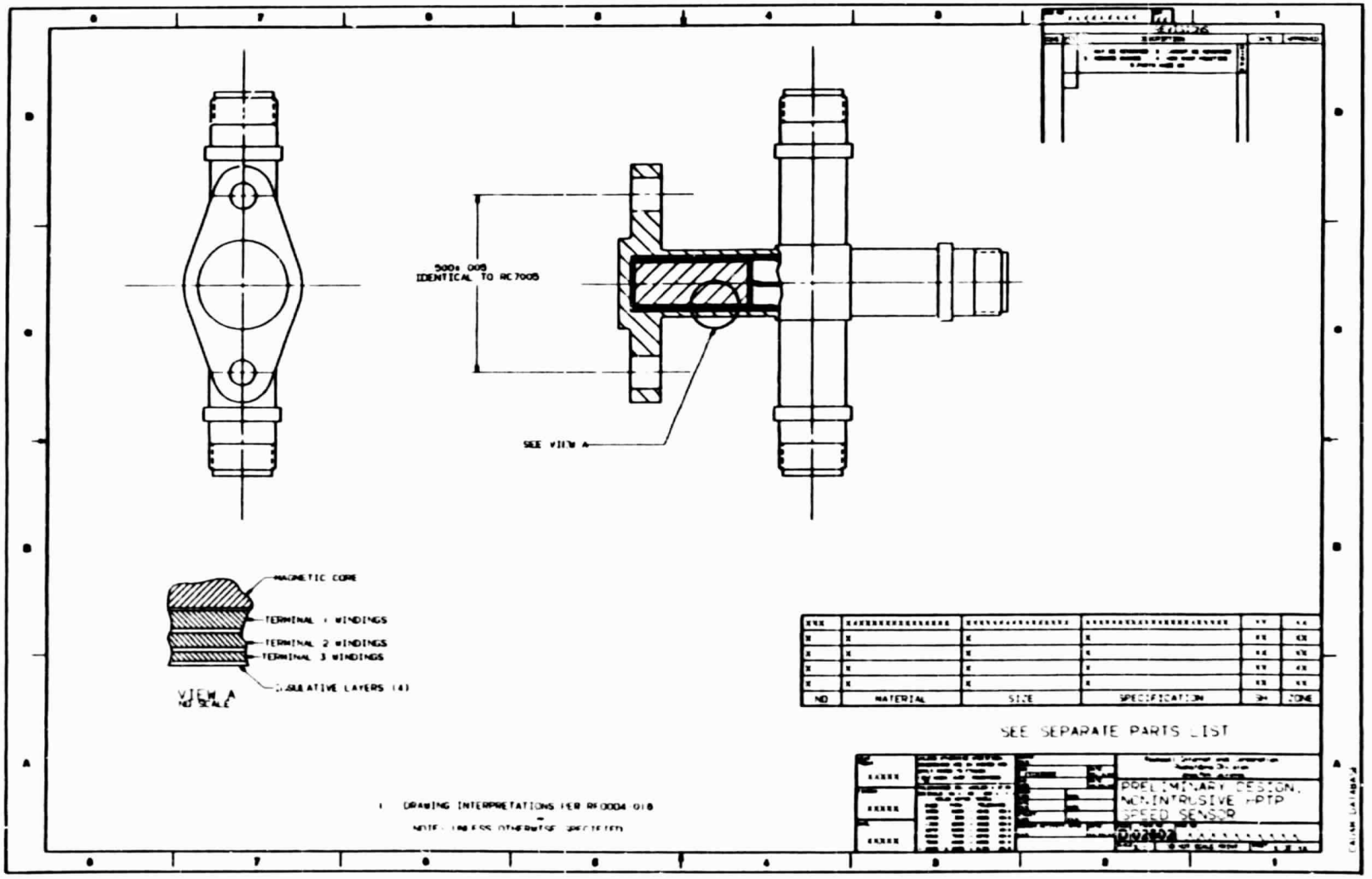

488-531

Rockwell International
Rocketdyne Division

Figure 22

TABLE 6

ELECTRICAL COMPONENTS FOR PRELIMINARY NON-INTRUSIVE SPEED SENSOR DESIGN

	EXISTING PROBE	EXPERIMENTAL CONFIGURATION	PRELIMINARY CONFIGURATION	COMMENTS
COIL TURNS	2400	1000	8000	
COIL SIZE	0.25 IN. DIA	0.875 x 0.875 IN.	0.47 IN. DIA	
WIRE GAGE	45	38	42	#42 COMMERCIALLY AVAILABLE
RESISTANCE	370 TO 1500 OHMS	84 OHMS	1530 OHMS	
INDUCTANCE	.01 TO 2.1 H	.018 H	0.172 H	0.172 H IS THE SATURATED INDUCTANCE
CORE SIZE	.060 IN. DIA	.375 x .375 IN.	.274 IN. DIA	
CORE MATERIAL	430 S.S.	HY-MU-80	HY-MU-80	ADDITIONAL CORE MATERIALS WILL BE INVESTIGATED DURING PHASE II
OUTPUT AMPLITUDE	>75mV*	9.5mV	76mV	75mV (PEAK) IS THE MINIMUM REQUIREMENT OF EXISTING CONTROLLER AT 600 RPM *RANGE TBD
SPEED	600 RPM	500 RPM	600 RPM	MINIMUM CONTROLLER REQUIREMENT
RESPONSE	3000 Hz	89,000 Hz	10,600 Hz	$F = (R + R_I)/2\pi L$, R_I = CONTROLLER INPUT RESISTANCE
GAP	0.030 IN.	3.5 IN.	3.5	

488-587A

Rockwell International
Rocketdyne Division

The preliminary design of the speed nut, the housing, and the electrical components indicated that all the elements of the variable-source magnetic speed sensor can be readily acquired and fabricated, providing a sensor meeting all the requirements of the RC7005 specifications.

PROGRAM SUMMARY/CONCLUSION

PHASE I

Phase I of the non-intrusive speed sensor program was completed within budget and ahead of schedule: the 12 months of tasks were completed in only 10 months. During the period, the following accomplishments were achieved:

Task I - Literature Search

Computerized literature searches were performed to identify published articles related to non-intrusive measurement techniques. These searches yielded 550 citations from which 42 article were obtained for review. Six new technologies were obtained from the search and supplemented the 8 technologies already known to us, resulting in 14 identified non-intrusive/remote speed sensing technologies.

Task II - Technology Evaluation

All 14 technologies were subjected to thorough theoretical evaluation to quantify their performance characteristics. Based upon the calculations of anticipated signal levels and environmental compatibilities, three promising technologies emerged from the analysis and were recommended for experimental evaluation: the variable-source magnetic approach, the infrared approach, and the microwave approach.

Task III - Experimental Evaluation

The variable-source magnetic speed sensor was tested in the laboratory to

determine the output signal amplitude at low speeds and large coil/magnet separations. Strong output signals were achieved by inserting rare-earth permanent magnets in the speed nut, by increasing the coil area and number of turns, and by introducing a high permeability core material into the coil: a 9.5 mV signal was achieved at 600 rpm and a 3.5-inch separation using samarium-cobalt magnets and a 1000-turn 7/8x7/8 inch coil with a HY-MU-80 core. Additional tests were performed to quantity the shielding effect of turbine blades and turbopump housing materials on the sensitivity of this new sensor. It was found that intervening Inconel 718 material had no noticeable attenuation effects on the sensor output signal up to 6000 rpm, which demonstrated the feasibility of mounting the variable-source magnetic speed sensor completely externally on the turbopump housing.

The infrared technology was tested for its immunity to attenuation effects from intervening cavitation (bubbles) in the liquid oxygen medium. The infrared cavitation experimentation determined the relative transmittance of visible and infrared light through a liquid medium with controllable levels of induced cavitation. It was found that, for bubbles of 0.01-0.5 centimeter radii, the liquid medium demonstrated very acceptable transmission characteristics for both visible and near-infrared light resulting in only 50% loss in transmission at the 6% cavitation level, in accordance with the Mie scattering calculations for these conditions. Confirmation of the feasibility of the visible/infrared approach would require an operating HPOTP under cryogenic and high pressure conditions.

The microwave technology must satisfy the same cavitation immunity requirements as the infrared technology. Our experiments indicated that nitrogen bubbles in liquid nonane only serve to change the cavity resonance modes of the waveguide, and have little or no signal attenuation effects on microwave energy transmittance. This technology must also prove itself on an operating HPOTP to verify its feasibility under cryogenic, high pressure conditions.

In short, all three of the technologies recommended on the basis of theoretical analysis have come through the experimental evaluation showing promise as viable speed sensing technologies.

Task IV - Tradeoff Analysis

Given that further experimental evaluation would be required to demonstrate the viability of the infrared and microwave technologies in the actual HPOTP operating environment, the variable-source magnetic speed sensor immediately presents itself as the candidate for preliminary design. This magnetic approach requires no controller modification and uses space-proven hardware, in addition to its inherent cavitation immunity. The possibility of mounting such a sensor completely outside the HPOTP makes the variable-source magnetic speed sensor a very attractive technology worthy of further development.

Task V - Preliminary Design

The preliminary design of the variable-source magnetic speed sensor was performed for the speed nut, probe, and electrical components. The proposed speed nut, which contains four magnets equally spaced around its periphery, was subjected to a preliminary stress analysis which indicated that magnets of sufficient size can be accommodated into the speed nut without adverse stress effects.

The preliminary probe design utilizes a modified sensor housing from the existing HPOTP speed sensor and removes the sensing elements to outside the liquid oxygen environment. This sensor uses the same mounting holes as the present speed sensor, thus requiring no modification of the HPOTP housing.

The preliminary design of the electrical components has resulted in a design which meets the controller requirements of 75mV minimum signal and 3000 Hz frequency response while increasing the probe gap from 0.030 to 3.5 inches.

In summary, the preliminary design task has indicated no obstacles in implementing the variable-source magnetic speed sensor approach.

RECOMMENDATION

It is recommended that Phase II be initiated immediately to fully develop the variable-source magnetic speed sensor for incorporation into the existing SSME HPOTP.

ACKNOWLEDGEMENTS

We gratefully acknowledge the direction of Tom Marshall and Harlan Burke for their help in overseeing this program, which was funded by NASA's Marshall Space Flight Center under contract number NAS8-34658. We additionally recognize the support of George Kuhr, John Collins, and Donald Hunter of Rocketdyne in the theoretical analysis and experimental verification of the variable-source speed sensor. We would also like to thank Dr. Ira Goldberg and Dr. Jim Rode of Rockwell International/Science Center for their consultation on the experimental evaluation of the microwave and infrared speed sensors.

BIBLIOGRAPHY

The following list of articles and reports generated as a result of the literature survey and utilized in the Theoretical Analysis serves as a useful bibliography on the state of the art in non-intrusive speed sensors.

"Wiegand Effect: A New Pulse-Generating Option", Automotive Engineering, 86(2), February 2, 1978, pp. 44-48.

Bhartia, P. and M. A. K. Hamid, "Doppler Radar Determination of the Rotation Speed of Shafts, "IEEE Trans. Ind. Electronics and Control Instrumentation, V. IECI-24, No. 1 (1977) p. 141.

Bucurenciu, S., "Dynamic Behavior of the Induction Tachometer", Rev Roum Sci Tech Electrotech Energ 25(2) (1980) p. 149.

Gadrault, R., "Shaft Rotation Speed Measurement Device, Its Checking and Variations Checking", (U.S. Patent) February 25, 1976

Hamilton, D. B. et al., Non-contact Devices for Measuring Vibrations and Deflections of Parts in Operating Turbopumps, Final Report, NASA CR124208.

Handlykken, M. B., "A Brushless D.C. Tachometer", (U.S. Patent) February 19, 1982.

Knoll, G. F., Radiation Detection and Measurement, Wiley, New York (1979), p. 504.

Macek, W., Electromagnetic Angular Rotation Sensing, Sperry Gyroscope Company Report, August 1964.

Noble, G. T., "Sensing Shaft Rotation With Proximity Switches, "Power Transmission Des., 25(10), August 10, 1981, pp. 62-63.

Parmenov, V. I., Angular Velocity and Acceleration Pick UP, Foreign Tech. Div. Air Force Systems Command, Wright-Patterson AFB, May 26, 1964.

Transandote, A. et al., "A New Slip Monitor for Traction Equipment", Trans. of the ASAE (1977), p. 851.

Verdrunes, M. and W. E. Mace, "The Measurement of Engine Rotational Speed", AGARD Flight Test Instrumentation Series, V. 4 (1973).

Wilcox, G. and J. L. Mason, "Temperature Stabilized Tachometer for the Fuel Efficient Automobile, "IEEE Trans. Consum. Electron, CE-26(3), August 3, 1980, pp. 664-669

A more detailed bibliography on non-intrusive/remote speed sensor technologies was presented in the Non-intrusive Speed Sensor Monthly Report to NASA/MSFC for February 1984 (NASA Contract NAS8-34658).